One molecule to couple them all: Towards realistic numbers of molecules in multiscale Molecular Dynamics simulations of exciton-polaritons

Ilia Sokolovskii,[1] Dmitry Morozov,[1] and Gerrit Groenhof[1]
Nanoscience Center and Department of Chemistry, University of Jyväskylä, P.O. Box 35, 40014 Jyväskylä, Finland.

(*Electronic mail: gerrit.x.groenhof@jyu.fi)

(*Electronic mail: ilia.i.sokolovskii@jyu.fi)

(Dated: 12 September 2024)

Collective strong coupling of many molecules to the confined light modes of an optical resonator can influence the photochemistry of these molecules, but the origin of this effect is not yet fully understood. To provide atomistic insights, several approaches have been developed based on quantum chemistry or molecular dynamics methods. However, most of these methods rely on coupling a few molecules (or sometimes only one) to a single cavity mode. To reach the strong coupling regime with such small number of molecules, much larger vacuum field strengths are employed than in experiments. To keep the vacuum field realistic and avoid potential artefacts, the number of coupled molecules should be significantly increased instead, but that is not always possible due to restrictions on computational hard- and software. To overcome this barrier and model the dynamics of an arbitrarily large ensemble of molecules coupled to realistic cavity fields in atomistic molecular dynamics simulations, we propose to coarse-grain subsets of molecules into one or more effective supermolecules with an enhanced dipole moment and concerted dynamics. To verify the validity of the proposed multiscale model, we performed simulations in which we investigated how the number of molecules that are coupled to the cavity, affects excited-state intra-molecular proton transfer, polariton relaxation and exciton transport.

I. INTRODUCTION

For over a decade, experiments on molecules in Fabry-Pérot cavities have suggested changes to their reactivity in ground or excited states.[1–7] While these changes have been attributed to hybridization of the confined light modes of the cavity and the excitations of the molecules into polaritons due to strong light-matter coupling,[8–10] there is no consensus on why such hybridization would change the chemistry. In particular, because the large majority of states that form are *dark*, meaning that they lack cavity mode contributions and hence should remain largely unaffected and thus similar to the uncoupled molecular states.[11–13] Furthermore, attempts at reproducing seminal experiments have either met with failure,[14,15] or revealed that the previous observations may have more trivial explanations that do not require polaritonic effects.[16,17] Because of these controversies, in combination with a lack of a theoretical model that can consistently account for *all* relevant aspects of strong light-matter coupling, the field of polaritonic chemistry, which aims at using optical resonators as catalysts for controlling chemistry,[18] has arrived at a pivotal stage. To push the field beyond that point, predictive models are required that consistently account for both the chemical details of the material and the mode structure of the electromagnetic fields inside the cavity.

Traditional quantum optics models, such as the Jaynes-Cummings model,[19,20] provide important conceptual insights into the effect of strong coupling on absorption spectra,[21] but without the atomistic details of the molecules, or the mode structure of the cavity, these models cannot predict how the cavity affects the physico-chemical properties of a material. To overcome this limitation, quantum optics models have been merged with quantum chemistry,[22–31] but because of the huge computational costs required for solving the electronic Schrödinger equation, these attempts have been mostly restricted to modeling a *single* molecule interacting with a *single* confined light mode. To compensate for the lack of the collective coupling strength provided by 10^5-10^8 molecules,[32–34] the cavity vacuum field strengths in such calculations were made significantly larger than in real Fabry-Pérot cavities, which could introduce artefacts.

To go beyond the single molecule / single cavity mode limitation and account for the interaction of *many* molecules with *multiple* modes of a Fabry-Pérot micro-cavity in atomistic computer simulations of polaritons, we had combined the multi-mode Tavis-Cummings model[35] with our own hybrid Quantum Mechanics / Molecular Mechanics (QM/MM) non-adiabatic molecular dynamics (MD) methodology for excited-state dynamics in proteins.[36,37] Through extensive parallelization of this model in GROMACS,[38] we could demonstrate that the molecular details matter, and that in particular molecular vibrations are essential for understanding how exciton transport,[39,40] excited-state relaxation,[41] or photo-chemistry[13] change under collective strong light-matter coupling. However, in spite of the efficient parallelism, the number of molecules that were included in our simulations, are still two to three orders of magnitude smaller than in experiments on microcavities, and the agreement with experiment were thus *qualitative* at best. To also achieve *quantitative* agreement with experiments, and make accurate predictions, polariton simulations should include as many molecules as in experiment, which currently is not possible.

To break this barrier and simulate an experimentally meaningful number of molecules coupled to realistic cavity vacuum fields, we propose a coarse-graining approach, in which we maintain an atomistic description for a sufficiently large num-

ber of molecules, while combining all other molecules into "supermolecules". The dynamics of the M molecules comprising such supermolecule, are thus assumed to be synchronized (ensemble coherence), which in the limit of very many molecules (N_{tot}) becomes a reasonable approximation.[42] With their enhanced dipole moments, each of these supermolecules provides the collective coupling strength of M molecules and hence interacts $\sqrt{M}$ times more strongly with the cavity vacuum field, which can therefore be reduced to realistic strengths in the simulations. Furthermore, these supermolecules effectively increase the density of dark states, which is essential for a correct description of the population dynamics between the bright and dark state manifolds in the larger ensembles we aim to model.[41] While previous works had introduced different effective-molecule approaches for avoiding the steep rise of the computational effort in modeling polaritons,[12,42–47] these approaches were based either on a simplified description of the molecules, or on a mean-field description of collective effects. In contrast, our approach retains an atomistic description for all molecules including their chemical environments, which we deem necessary for a consistent description of the molecular dynamics under strong light matter coupling.

The article is organised in the following way: In Sec. II, we explain the theory underlying the coarse-graining approach. In Sec. III, we provide the details and parameters of atomistic simulations of the molecular-cavity systems used in the article, and we then present and discuss the results of these simulations in Sec. IV. In Sec. V, we conclude the article with a short summary and an outlook.

II. THEORETICAL BACKGROUND

Within the Born-Oppenheimer approximation for electronic strong coupling,[48,49] we separate the nuclear motion, which we describe classically, from the electronic *plus* cavity mode degrees of freedom, which we model with quantum mechanics. For a *single* molecule, the interaction between the electronic degrees of freedom, here the electronic ground (S_0) and excited states (S_1) of the molecule, on the one hand, and a *single* cavity mode on the other hand, is described within the long-wavelength approximation by the established Rabi Hamiltonian:

$$\begin{aligned}\hat{H}^{\mathrm{Rabi}} &= h\nu(\mathbf{R})\hat{\sigma}^{+}\hat{\sigma}^{-} + \hbar\omega_{\mathrm{cav}}\hat{a}^{\dagger}\hat{a} + \\ &\quad \boldsymbol{\mu}(\mathbf{R})\left[\hat{\sigma}^{+}+\hat{\sigma}^{-}\right]\cdot\left[\mathbf{E}^{*}(\mathbf{R}_c)\hat{a}^{\dagger}+\mathbf{E}(\mathbf{R}_c)\hat{a}\right] + V_{\mathrm{S}_0}(\mathbf{R}).\end{aligned} \tag{1}$$

Here, operator $\hat{\sigma}^{+} = |\mathrm{S}_1\rangle\langle\mathrm{S}_0|$ excites the molecule from the singlet electronic ground state (S_0) with energy $V_{\mathrm{S}_0}(\mathbf{R})$, to the first singlet electronic excited state (S_1) with energy $V_{\mathrm{S}_1}(\mathbf{R})$; operator $\hat{\sigma}^{-} = |\mathrm{S}_0\rangle\langle\mathrm{S}_1|$ de-excites the molecule from S_1 to S_0; $h\nu(\mathbf{R}) = V_{\mathrm{S}_1}(\mathbf{R}) - V_{\mathrm{S}_0}(\mathbf{R})$ is the excitation energy of the molecule; $\mathbf{R}$ is the vector of nuclear coordinates of the molecule; operators $\hat{a}^{\dagger}$ and $\hat{a}$ create and annihilate a cavity photon of energy $\hbar\omega_{\mathrm{cav}}$, respectively; $\boldsymbol{\mu}(\mathbf{R})$ is the transition dipole moment of the molecule; and $\mathbf{E}(\mathbf{R}_c)$ is the electric component of the vacuum field associated with the cavity mode at the geometric center of the molecule, $\mathbf{R}_c$.

Within the rotating wave approximation (RWA), valid below the ultra-strong coupling limit (*i.e.*, when $\boldsymbol{\mu}(\mathbf{R})\cdot\mathbf{E}(\mathbf{R}_c) < 0.1\, h\nu(\mathbf{R})$),[50] this equation simplifies to the Jaynes-Cummings Hamiltonian of quantum optics:[19]

$$\begin{aligned}\hat{H}^{\mathrm{JC}}_{\mathrm{RWA}} &= h\nu(\mathbf{R})\hat{\sigma}^{+}\hat{\sigma}^{-} + \hbar\omega_{\mathrm{cav}}\hat{a}^{\dagger}\hat{a} + \\ &\quad \boldsymbol{\mu}(\mathbf{R})\cdot\left[\mathbf{E}(\mathbf{R}_c)\hat{\sigma}^{+}\hat{a} + \mathbf{E}^{*}(\mathbf{R}_c)\hat{\sigma}^{-}\hat{a}^{\dagger}\right] + V_{\mathrm{S}_0}(\mathbf{R}).\end{aligned} \tag{2}$$

Solving the eigenvalue problem for the Hamiltonian in equation 2 yields two eigenstates, which are conventionally called the lower (LP) and upper (UP) polaritonic states:

$$|\psi^{\mathrm{LP/UP}}\rangle = \beta^{\mathrm{LP/UP}}\hat{\sigma}^{+}|\phi_0\rangle + \alpha^{\mathrm{LP/UP}}\hat{a}^{\dagger}|\phi_0\rangle, \tag{3}$$

where $|\phi_0\rangle$ is the ground state of the molecule-cavity system with no excitation in neither the molecule nor the cavity mode. The $\beta^{\mathrm{LP/UP}}$ and $\alpha^{\mathrm{LP/UP}}$ expansion coefficients give the contributions of the molecular and the cavity mode excitations, respectively, to polaritonic state $|\psi^{\mathrm{LP/UP}}\rangle$.[21,51] Unless stated otherwise, we will assume resonance between the molecular excitation and the caviy mode, *i.e.*, $h\nu(\mathbf{R}) = \hbar\omega_{\mathrm{cav}}$. Under such conditions, the magnitudes of the expansion coefficients are equal, $|\beta^{\mathrm{LP/UP}}|^2 = |\alpha^{\mathrm{LP/UP}}|^2 = 0.5$, and the Rabi splitting between the LP and UP is

$$\hbar\Omega^{1}_{\mathrm{R}} = 2\hbar\boldsymbol{\mu}(\mathbf{R})\cdot\mathbf{u}_{\mathrm{cav}}\sqrt{\frac{\hbar\omega_{\mathrm{cav}}}{2\varepsilon_0 V_{\mathrm{cav}}}} \tag{4}$$

where $\mathbf{u}_{\mathrm{cav}}$ is the unit vector of the electric component of the cavity vacuum field; ε_0 the dielectric constant; and V_{cav} the cavity mode volume. The superscript 1 in $\hbar\Omega^{1}_{\mathrm{R}}$ implies that the strong coupling is for a single molecule. In further derivations, we will omit the LP and UP labels. The adiabatic potential energy surfaces associated with the polaritonic states are obtained as the expectation value of $\hat{H}^{\mathrm{JC}}_{\mathrm{RWA}}$:

$$\begin{aligned}V(\mathbf{R}) &= \langle\psi|\hat{H}^{\mathrm{JC}}_{\mathrm{RWA}}|\psi\rangle = \\ &\quad |\beta|^2 V_{\mathrm{S}_1}(\mathbf{R}) + |\alpha|^2\left[V_{\mathrm{S}_0}(\mathbf{R}) + \hbar\omega_{\mathrm{cav}}\right] + \\ &\quad \beta^{*}\alpha\boldsymbol{\mu}(\mathbf{R})\cdot\mathbf{E}(\mathbf{R}_c) + \alpha^{*}\beta\boldsymbol{\mu}(\mathbf{R})\cdot\mathbf{E}^{*}(\mathbf{R}_c).\end{aligned} \tag{5}$$

The Hamiltonian in equation 2 can be extended to an ensemble of N_{tot} molecules interacting with the same confined light mode, resulting in the Tavis-Cummings Hamiltonian:[20]

$$\begin{aligned}\hat{H}^{\mathrm{TC}} &= \sum_{j}^{N_{\mathrm{tot}}} h\nu_j(\mathbf{R}_j)\hat{\sigma}^{+}_j\hat{\sigma}^{-}_j + \hbar\omega_{\mathrm{cav}}\hat{a}^{\dagger}\hat{a} + \\ &\quad \sum_{j}^{N_{\mathrm{tot}}}\boldsymbol{\mu}_j(\mathbf{R}_j)\cdot\left[\mathbf{E}(\mathbf{R}^{j}_c)\hat{\sigma}^{+}_j\hat{a} + \mathbf{E}^{*}(\mathbf{R}^{j}_c)\hat{\sigma}^{-}_j\hat{a}^{\dagger}\right] + \sum_{j}^{N_{\mathrm{tot}}} V_{\mathrm{S}_0}(\mathbf{R}_j)\end{aligned} \tag{6}$$

where the indices j in the transition dipole moment and excitation energy indicate that these quantities are evaluated for

molecule j with atomic coordinates $\mathbf{R}_j$ and centered at $\mathbf{R}_c^j$. The eigenstates of the Tavis-Cummings Hamiltonian are

$$|\psi^m\rangle = \sum_j^{N_{\rm tot}} \beta_j^m \hat{\sigma}_j^+ |\phi_0\rangle + \alpha^m \hat{a}^\dagger |\phi_0\rangle \tag{7}$$

with $m = 0, 1, ..., N_{\rm tot}+1$. Without disorder and when all molecules are identical, two of these $N_{\rm tot}+1$ states have a 50 % contribution from the cavity mode and are therefore bright, while the remaining $N_{\rm tot}-1$ states are dark, with their name reflecting a negligible contribution of the cavity mode. The polaritonic potential energy surfaces for the $N_{\rm tot}$ molecule system contain contributions from each molecule:

$$\begin{aligned} V^m(\{\mathbf{R}\}) &= \langle\psi^m|\hat{H}^{\rm TC}|\psi^m\rangle = \\ &\sum_j^{N_{\rm tot}} |\beta_j^m|^2 \left[V_{\rm S_1}(\mathbf{R}_j) + \sum_{i\neq j}^{N_{\rm tot}} V_{\rm S_0}(\mathbf{R}_i)\right] + \\ &|\alpha^m|^2 \left[\sum_j^{N_{\rm tot}} V_{\rm S_0}(\mathbf{R}_j) + \hbar\omega_{\rm cav}(\mathbf{k}_z)\right] + \\ &\sum_j^{N_{\rm tot}} (\beta_j^m)^* \alpha^m \boldsymbol{\mu}_j(\mathbf{R}_j)\cdot\mathbf{E}(\mathbf{R}_c^j) + \\ &(\alpha^m)^* \sum_j^{N_{\rm tot}} \beta_j^m \boldsymbol{\mu}_j(\mathbf{R}_j)\cdot\mathbf{E}^*(\mathbf{R}_c^j) \end{aligned} \tag{8}$$

with $\{\mathbf{R}\}$ a radius-vector containing the coordinates of all $N_{\rm tot}$ molecules.

The collective Rabi splitting is proportional to the square root of the number of molecules in the mode volume, *i.e.*, $\hbar\Omega_{\rm R} = \hbar\Omega_{\rm R}^1\sqrt{N_{\rm tot}} \propto \sqrt{N_{\rm tot}/V_{\rm cav}}$. With typical transition dipole moments on the order of a few Debye, reaching the strong coupling regime to form polaritons with organic molecules in Fabry-Pérot cavities that have mode volumes on the order of $V_{\rm cav} \propto (\lambda_{\rm cav}/n_{\rm r})^3$ (where $\lambda_{\rm cav}$ is the wavelength of the cavity mode and $n_{\rm r}$ is the refractive index), requires collective coupling of many molecules, 10^5-10^8 (*e.g.*, see ref.[34,52,53]). Modeling that many molecules is intractable with today's computational resources. However, as we show below, if the molecules are all *identical*, the computational effort required for the evaluation of the potential energy surfaces can be reduced to that required when only a single molecule is strongly coupled.[42]

For M identical molecules without disorder, Equations 7 and 8 can be simplified to

$$\begin{aligned} |\psi_{(M)}^m\rangle &= \beta_{(M)}^m \textstyle\sum_j^M \hat{\sigma}_j^+ |\phi_0\rangle + \alpha^m \hat{a}^\dagger |\phi_0\rangle = \\ &\tfrac{1}{\sqrt{M}} \beta_{(1)}^m \textstyle\sum_j^M \hat{\sigma}_j^+ |\phi_0\rangle + \alpha^m \hat{a}^\dagger |\phi_0\rangle \end{aligned} \tag{9}$$

and

$$\begin{aligned} V_{(M)}^m(\{\mathbf{R}\}) &= |\beta_{(1)}^m|^2 \left[V_{\rm S_1}(\mathbf{R}) + (M-1)V_{\rm S_0}(\mathbf{R})\right] + \\ &|\alpha^m|^2 \left[M V_{\rm S_0}(\mathbf{R}) + \hbar\omega_{\rm cav}\right] + \\ &\sqrt{M}(\beta_{(1)}^m)^* \alpha^m \boldsymbol{\mu}(\mathbf{R})\cdot\mathbf{E}(\mathbf{R}_c) + \\ &\sqrt{M}(\alpha^m)^* \beta_{(1)}^m \boldsymbol{\mu}(\mathbf{R})\cdot\mathbf{E}^*(\mathbf{R}_c). \end{aligned} \tag{10}$$

Here, we introduced subscript "(M)" to indicate that we describe a system of M *identical* molecules. Likewise, we used the relation between the expansion coefficient $\beta_{(1)}^m$ of a single molecule coupled to a cavity mode, and the expansion coefficient $\beta_{(M)}^m$ of one of the M identical molecules that are coupled to the same cavity mode: $\beta_{(M)}^m = \beta_{(1)}^m/\sqrt{M}$. Therefore, $\sum_j^M (\beta_{(M)}^m)_j = \sum_j^M \beta_{(1)}^m/\sqrt{M} = \sqrt{M}\beta_{(1)}^m$. The full derivation of equations 8 and 10 is provided in the Supporting Information (SI, Section S1.1).

Keeping all molecules identical is, however, an oversimplification of reality, in which all molecules are different, in particular under ambient conditions. To nevertheless exploit the huge computational savings associated with keeping molecules identical,[42] we take inspiration from so-called coarse-graining approaches in biomolecular modeling, in particular the Martini force field,[54] in which several atoms, or even molecules are grouped together and treated as single entities to reduce the overall number of particles in the simulation. Such approaches have been successfully applied to perform MD simulations of biomolecular systems that are too large for a fully atomistic treatment, such as biological cells.[55] Here, to keep simulations with very large numbers of molecules, $N_{\rm tot}$, coupled to a cavity, tractable, we introduce a multi-scale approach, illustrated in Figure 1, in which we employ a coarse-grained description for $N_{\rm S}$ subsets of M molecules each, while maintaining a single molecule description for a sufficiently large number, N, of "normal" molecules.

The link between one and many identical molecules in Equations 9 and 10 can be generalized to the multi-scale situation with N "normal" molecules, which can be chemically identical, but have different geometries, and $N_{\rm S}$ coarse-grained "supermolecules", each of which representing $M = \frac{N_{\rm tot}-N}{N_{\rm S}}$ fully identical (for a particular supermolecule) molecules with the same structure and dynamics. First, we consider the situation when N normal molecules and a *single* supermolecule (*i.e.*, $N_{\rm S}=1$) that combines $M = N_{\rm tot}-N$ identical molecules, are coupled to a single cavity mode. The polaritonic eigenstates are

$$|\psi_{(N+1_{\rm S})}^m\rangle = \sum_i^N \beta_i^m \hat{\sigma}_i^+ |\phi_0\rangle + \beta_{\rm S}^m \hat{\sigma}_{N+1}^+ |\phi_0\rangle + \alpha^m \hat{a}^\dagger |\phi_0\rangle, \tag{11}$$

where we used subscript S in the molecular expansion coefficient $\beta_{\rm S}^m$ to emphasize that this coefficient belongs to the supermolecule. This coefficient is related to the expansion coefficient $\beta_{\rm norm}^m$ of the identical molecules that were coarse-grained into the supermolecules, via $\beta_{\rm S}^m = \sqrt{M}\beta_{\rm norm}^m$. The potential energy surfaces associated with these eigenstates are evaluated as

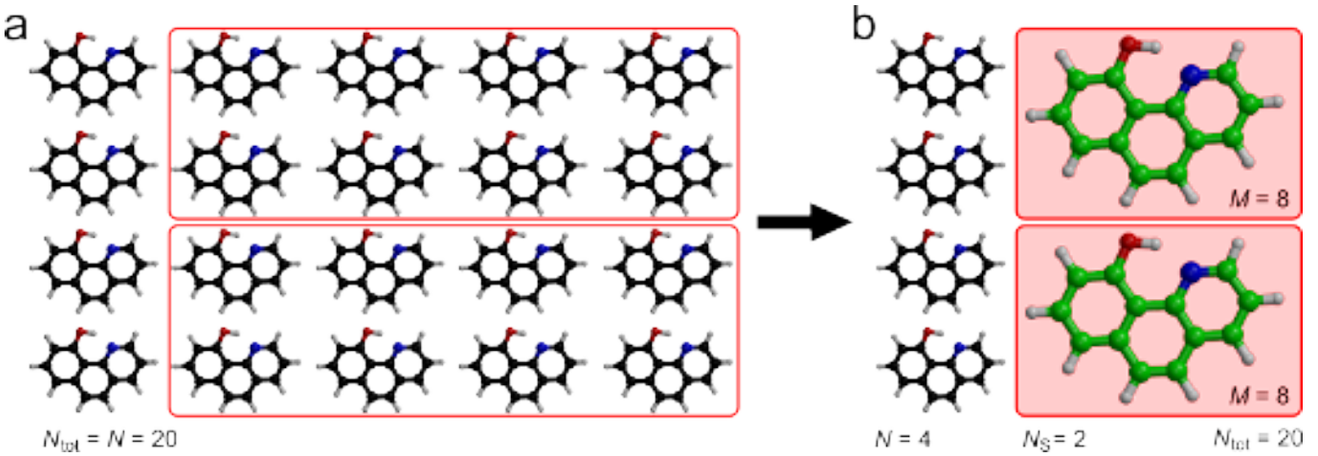

FIG. 1. Coarse-graining subsets of M molecules into N_S supermolecules. In (**a**), $N_{tot} = N = 20$ "normal" molecules (black carbons) are coupled to the cavity. In the coarse-grained representation, illustrated in (**b**), $N = 4$ molecules are kept normal, while $M = 8$ molecules are combined into $N_S = 2$ "supermolecules" (green carbons) with increased interaction strength of $g_S = \sqrt{M} g_1$, with $g_1 = \boldsymbol{\mu}_1 \cdot \mathbf{E}$ the coupling strength of a single molecule within the subset. Because of the scaled interaction strength of the supermolecules (illustrated by their larger sizes in **b**), the Rabi splitting still reflects the situation with $N_{tot} = 20$ molecules, whereas the number of molecules that needs to be described explicitly, is reduced to $N + N_S = 6$, significantly saving computer resources.

$$\begin{aligned} V^m_{(N+1_S)}(\mathbf{R}) &= \textstyle\sum_i^N |\beta_i^m|^2 \left[V_{S_1}(\mathbf{R}_i) + \sum_{j\neq i}^N V_{S_0}(\mathbf{R}_j) + M V_{S_0}(\mathbf{R}_{N+1})\right] + |\beta_S^m|^2 \left[\sum_i^N V_{S_0}(\mathbf{R}_i) + V_{S_1}(\mathbf{R}_{N+1}) + (M-1) V_{S_0}(\mathbf{R}_{N+1})\right] + \\ & |\alpha^m|^2 \left[\sum_i^N V_{S_0}(\mathbf{R}_i) + M V_{S_0}(\mathbf{R}_{N+1}) + \hbar\omega_{cav}\right] + \sum_i^N \boldsymbol{\mu}_i(\mathbf{R}_i) \cdot \left[(\beta_i^m)^* \alpha^m \mathbf{E}(\mathbf{R}_c^i) + (\alpha^m)^* \beta_i^m \mathbf{E}^*(\mathbf{R}_c^i)\right] + \\ & \sqrt{M} \boldsymbol{\mu}_{N+1}(\mathbf{R}_{N+1}) \left[(\beta_S^m)^* \alpha^m \mathbf{E}(\mathbf{R}_c^{N+1}) + (\alpha^m)^* \beta_S^m \mathbf{E}^*(\mathbf{R}_c^{N+1})\right] \end{aligned} \tag{12}$$

For the more general situation with N normal molecules and N_S supermolecules ($N + N_S$), each composed of M identical molecules, the eigenstates of the Tavis Cummings Hamiltonian are

$$|\psi^m_{(N+N_S)}\rangle = \sum_i^N \beta_i^m \hat{\sigma}_i^+ |\phi_0\rangle + \sum_l^{N_S} \beta_{S,l}^m \hat{\sigma}_{N+l}^+ |\phi_0\rangle + \alpha^m \hat{a}^\dagger |\phi_0\rangle, \tag{13}$$

and potential energy surfaces associated with these states are

$$\begin{aligned} V^m_{(N+N_S)}(\mathbf{R}) &= \textstyle\sum_i^N |\beta_i^m|^2 \left[V_{S_1}(\mathbf{R}_i) + \sum_{j\neq i}^N V_{S_0}(\mathbf{R}_j) + M \sum_l^{N_S} V_{S_0}(\mathbf{R}_{N+l})\right] + \\ & \sum_l^{N_S} |\beta_{S,l}^m|^2 \left[\sum_i^N V_{S_0}(\mathbf{R}_i) + V_{S_1}(\mathbf{R}_{N+l}) + (M-1) V_{S_0}(\mathbf{R}_{N+l}) + M \sum_{q\neq l}^{N_S} V_{S_0}(\mathbf{R}_{N+q})\right] + \\ & |\alpha^m|^2 \left[\sum_i^N V_{S_0}(\mathbf{R}_i) + M \sum_l^{N_S} V_{S_0}(\mathbf{R}_{N+l}) + \hbar\omega_{cav}\right] + \\ & \sum_i^N \boldsymbol{\mu}_i(\mathbf{R}_i) \cdot \left[(\beta_i^m)^* \alpha^m \mathbf{E}(\mathbf{R}_c^i) + (\alpha^m)^* \beta_i^m \mathbf{E}^*(\mathbf{R}_c^i)\right] + \\ & \sqrt{M} \sum_l^{N_S} \boldsymbol{\mu}_{N+l}(\mathbf{R}_{N+l}) \left[(\beta_{S,l}^m)^* \alpha^m \mathbf{E}(\mathbf{R}_c^{N+l}) + (\alpha^m)^* \beta_{S,l}^m \mathbf{E}^*(\mathbf{R}_c^{N+l})\right] \end{aligned} \tag{14}$$

These results can be further extended to describe strong coupling between N normal molecules and N_S supermolecules on the one hand, and *multiple* cavity modes on the other hand, yielding the following expression for the eigenstates:

$$\begin{aligned} |\psi^m_{(N+N_S)}\rangle &= \textstyle\sum_i^N \beta_i^m \hat{\sigma}_i^+ |\phi_0\rangle + \sum_l^{N_S} \beta_{S,l}^m \hat{\sigma}_{N+l}^+ |\phi_0\rangle + \\ & \textstyle\sum_p^{n_{modes}} \alpha_p^m \hat{a}_p^\dagger |\phi_0\rangle, \end{aligned} \tag{15}$$

where the number of the cavity modes n_{modes} is in principle infinite. To make the computations feasible, we apply periodic boundary conditions in the in-plane direction (*i.e.*, $\mathbf{E}(z) = \mathbf{E}(z+L_z)$, with L_z the length of the one-dimensional cavity), which quantizes the wave vector $\mathbf{k}_z$ to discrete values, $k_{z,p} = 2\pi p/L_z$, and employ a cut-off on the cavity dispersion, $\hbar\omega(k_{z,p_{\max}})$, such that $p_{\max} = n_{\text{modes}}$.[35]

With this approximation, the potential energy surface of polaritonic state ψ^m for a system of N normal and N_S supermolecules coupled to n_{modes} cavity modes is evaluated as:[38]

$$\begin{aligned}
V^m_{(N+N_S)}(\mathbf{R}) \;=\; & \textstyle\sum_i^N |\beta_i^m|^2 \left[V_{S_1}(\mathbf{R}_i) + \sum_{j\neq i}^N V_{S_0}(\mathbf{R}_j) + M\sum_l^{N_S} V_{S_0}(\mathbf{R}_{N+l})\right] + \\
& \textstyle\sum_l^{N_S} |\beta_{S,l}^m|^2 \left[\sum_i^N V_{S_0}(\mathbf{R}_i) + V_{S_1}(\mathbf{R}_{N+l}) + (M-1)V_{S_0}(\mathbf{R}_{N+l}) + M\sum_{q\neq l}^{N_S} V_{S_0}(\mathbf{R}_{N+q})\right] + \\
& \textstyle\sum_p^{n_{\text{modes}}} |\alpha_p^m|^2 \left[\sum_i^N V_{S_0}(\mathbf{R}_i) + M\sum_l^{N_S} V_{S_0}(\mathbf{R}_{N+l}) + \hbar\omega_{\text{cav}}(\mathbf{k}_{z,p})\right] + \\
& \textstyle\sum_i^N \sum_p^{n_{\text{modes}}} \boldsymbol{\mu}_i(\mathbf{R}_i)\cdot\left[(\beta_i^m)^*\alpha_p^m\mathbf{E}_p(\mathbf{R}_c^i) + (\alpha_p^m)^*\beta_i^m\mathbf{E}_p^*(\mathbf{R}_c^i)\right] + \\
& \sqrt{M}\textstyle\sum_l^{N_S}\sum_p^{n_{\text{modes}}} \boldsymbol{\mu}_{N+l}(\mathbf{R}_{N+l})\left[(\beta_{S,l}^m)^*\alpha_p^m\mathbf{E}_p(\mathbf{R}_c^{N+l}) + (\alpha_p^m)^*\beta_{S,l}^m\mathbf{E}_p^*(\mathbf{R}_c^{N+l})\right]
\end{aligned} \tag{16}$$

Here, we replaced the cavity mode energy by the cavity dispersion, which for a Fabry-Pérot cavity is

$$\hbar\omega_{\text{cav}}(k_z) = \hbar\sqrt{\omega_0^2 + c^2k_z^2/n_r^2} \tag{17}$$

with c is the speed of light; k_z the in-plane momentum of the confined light mode and $\hbar\omega_0$ the energy of the fundamental cavity mode with zero in-plane momentum. In addition, we introduced subscripts in $\mathbf{E}_p$ to indicate that each mode has its own cavity vacuum field.

To compute semi-classical MD trajectories of the N normal molecules plus M supermolecules, the Hellman-Feynman gradients ($\langle\psi^k|\nabla_a\hat{H}^{\text{TC}}|\psi^m\rangle$) between eigenstates $|\psi^k\rangle = |\psi^k_{(N+N_S)}\rangle$ and $|\psi^m\rangle = |\psi^m_{(N+N_S)}\rangle$ are required. For an atom a that is a part of molecule l, these gradients are computed as

$$\begin{aligned}
\langle\psi^k|\nabla_{a\in l}\hat{H}^{\text{TC}}|\psi^m\rangle \;=\; & (\beta_l^k)^*\beta_l^m\nabla_{a\in l}V_{S_1}(\mathbf{R}_l) + \left[\delta_{km} - (\beta_l^k)^*\beta_l^m\right]\nabla_{a\in l}V_{S_0}(\mathbf{R}_l) - \\
& (\beta_l^k)^*\textstyle\sum_p^{n_{\text{modes}}}\alpha_p^m\nabla_{a\in l}\boldsymbol{\mu}_l(\mathbf{R}_l)\cdot\mathbf{E}_p(\mathbf{R}_c^l) - \sum_p^{n_{\text{modes}}}(\alpha_p^m)^*\beta_l^k\nabla_{a\in l}\boldsymbol{\mu}_l(\mathbf{R}_l)\cdot\mathbf{E}_p^*(\mathbf{R}_c^l),
\end{aligned} \tag{18}$$

if molecule l is a normal molecule, and as

$$\begin{aligned}
\langle\psi^k|\nabla_{a\in l}\hat{H}^{\text{TC}}|\psi^m\rangle \;=\; & (\beta_{S,l}^k)^*\beta_{S,l}^m\left[\nabla_{a\in l}V_{S_1}(\mathbf{R}_{N+l}) + (M-1)\nabla_{a\in l}V_{S_0}(\mathbf{R}_{N+l})\right] + \\
& M\left[\delta_{km} - (\beta_{S,l}^k)^*\beta_{S,l}^m\right]\nabla_{a\in l}V_{S_0}(\mathbf{R}_{N+l}) - \\
& \sqrt{M}(\beta_{S,l}^k)^*\textstyle\sum_p^{n_{\text{modes}}}\alpha_p^m\nabla_{a\in l}\boldsymbol{\mu}_{N+l}(\mathbf{R}_{N+l})\cdot\mathbf{E}_p(\mathbf{R}_c^{N+l}) - \\
& \sqrt{M}\sum_p^{n_{\text{modes}}}(\alpha_p^m)^*\beta_{S,l}^m\nabla_{a\in l}\boldsymbol{\mu}_{N+l}(\mathbf{R}_{N+l})\cdot\mathbf{E}_p^*(\mathbf{R}_c^{N+l}),
\end{aligned} \tag{19}$$

if molecule l is a supermolecule. In the latter case, the forces are evenly distributed over the M molecules that comprise the supermolecule, such that their dynamics are identical (SI, section 3.1). In addition to the derivatives in the adiabatic basis of the eigenstates of the Tavis-Cummings Hamiltonian (equations 18 and 19), we also provide a derivation for the gradients in the diabatic basis of product states between molecular and cavity mode excitations in the SI (section S1.2).

III. SIMULATION DETAILS

To verify if the dynamics remain consistent when we coarse-grain subsets of molecules into supermolecules, we have repeated MD simulations that were previously done with fewer molecules and artificially strong vacuum fields, for a larger effective number of molecules (N_{tot}) and a smaller, and hence more realistic, vacuum field. We specifically focused on the following processes:

1. Excited-state intra-molecular proton transfer (ESIPT)

reaction of 10-hydroxybenzo[h]quinoline (HBQ, Figure 2a) molecules coupled to a single-mode cavity;[13]

2. Population dynamics in a system of Rhodamine molecules (Figure 2b) coupled to a single-mode cavity;[56] and

3. Polariton transport in a multi-mode Fabry-Pérot cavity containing Rhodamine molecules.[39]

All simulations were carried out with GROMACS 4.5.3,[57] which for processes 1 and 2 was interfaced to TeraChem,[58,59] and to Gaussian16 for process 3.[60] In these simulations, the total polaritonic wave function was expanded as a linear combination of diabatic light-matter states,

$$|\Psi(t)\rangle = \sum_{j}^{N+N_S+n_{\text{modes}}} |\phi_j\rangle d_j(t), \tag{20}$$

where basis function $|\phi_j\rangle$ represents a state with either one of the molecules (j) in the S_1 electronic excited state whilst all other molecules are in the S_0 electronic ground state, and no photons in the cavity, *i.e.*, $|\phi_j\rangle = \hat{\sigma}_j^+ |\Pi_i^N S_0^i\rangle \otimes |\Pi_p^{n_{\text{modes}}} 0_p\rangle$, or all molecules in the ground state with one cavity mode (with index j) excited, *i.e.*, $|\phi_{j>N+N_S}\rangle = \hat{a}^\dagger_{j-(N+N_S)} |\Pi_i^N S_0^i\rangle \otimes |\Pi_p^{n_{\text{modes}}} 0_p\rangle$. The diabatic expansion coefficients $d_j(t)$ were propagated with a unitary propagator, while the nuclear degrees of freedom were evolved on adiabatic polaritonic potential energy surfaces associated with the eigenstates of the Tavis Cummings Hamiltonian.[61] To model the non-adiabatic population transfer between the adiabatic eigenstates, we used the fewest-switches surface hopping algorithm for processes 1 and 2, and the Ehrenfest mean-field approach for process 3. Cavity decay was treated by adding the losses explicitly to the Hamiltonian, whereas molecular decay was neglected. The justification for the latter assumption is the much longer radiative lifetime of the molecules (nanoseconds) compared to the metallic Fabry-Pérot cavities typically used in experiments (femtoseconds).[32] The details of the implementation of the method in GROMACS can be found elsewhere.[23,38,61] Below, we elaborate on the setup of the molecule-cavity systems and share the details of the molecular models employed in the simulations.

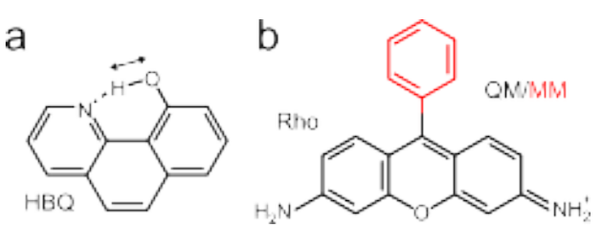

FIG. 2. Molecules modelled in this work: (**a**) 10-hydroxybenzo[h]quinoline (HBQ) chromophore, which upon excitation into the first singlet excited electronic state (S_1) undergoes ultra-fast proton transfer from the O to N atom (double-headed arrow); (**b**) Rhodamine (Rho) fluorophore, described at the QM/MM level with the QM subsystem in black and the MM subsystem in red. For clarity, aromatic hydrogens and solvent molecules are omitted.

A. Molecular dynamics model systems

1. *HBQ molecule in cyclohexane*

A single HBQ molecule (Figure 2a), with a geometry optimized at the CAM-B3LYP/6-31G(d) level of theory, was placed at the center of a rectangular periodic box, to which 402 cyclohexane molecules were added, yielding 2435 atoms in total. The interactions in this system were modeled with the Gromos-2016H66 force field.[62] For computing the Van der Waals interactions between HBQ and the cyclohexane molecules, the following Gromos96 atom-types were used: `HC` for all aromatic hydrogen atoms, `C` for all carbon atoms, `NR` for the aromatic nitrogen atom, `OA` for the hydroxyl oxygen atom and `H` for the hydroxyl proton. These interactions were described with a Lennard-Jones potential that was truncated at 1.4 nm. The cyclohexane solvent was equilibrated for 100 ns with the coordinates of the HBQ atoms fixed. The bond lengths in cyclohexane were constrained with the LINCS algorithm,[63] which enabled a time step of 2 fs. Constant temperature (300 K) and pressure (1 atmosphere) were maintained by weakly coupling to an external bath ($\tau_T = 0.1$ ps, $\tau_P = 1$ ps).[64]

We extracted snapshots from the equilibration trajectory and further equilibrated the simulation box for 50 ps at the QM/MM level with a time step of 1 fs and without constraints on the positions of the HBQ atoms. In these simulations, HBQ was modeled at the QM level, using density functional theory (DFT) in combination with the CAM-B3LYP exchange-correlation functional[65–67] and the 6-31G(d) basis set.[68]. This QM subsystem was mechanically embedded within the MM subsystem, consisting of the cyclohexane molecules. The cyclohexane molecules and their interactions with HBQ were again described with the Gromos2016H66 force field.[62] To model the first singlet electronic excited (S_1) state of HBQ, we employed time-dependent DFT (TD-DFT)[69] within the Tamm-Dancoff approximation[70] (TDA) in combination with the CAM-B3LYP functional and the 6-31G(d) basis set.

2. *Rhodamine molecule in water*

An equilibrated simulation box of Rhodamine in water was taken from Luk *et al.*[23] In this system, the Rhodamine molecule was described at the QM/MM level with the fused rings system (black, Figure 2b) in the QM region, and the rest of the molecule plus the water in the MM region (red, Figure 2b). The QM subsystem was modelled at the Restricted Hartree-Fock (RHF)/3-21G level of theory in the ground state (S_0) and at the Configuration Interaction method, truncated at single electron excitations (CIS) in the electronic excited state (S_1). The rest of the molecule as well as the water solvent were modelled with the Amber03 force field[71] and TIP3P water model,[72] respectively. The bond between the QM and MM subsystems was replaced by a constraint. The QM part was capped with a hydrogen atom, and the force on this atom was distributed over the QM and MM atoms of the bond. The QM system interacted with the Coulomb field of all MM atoms

within a 1.6 nm cut-off sphere. Lennard-Jones interactions between the QM and all MM atoms within a 1.0 nm were added. Prior to the simulations of the Rhodamine cavity systems, we equilibrated the Rhodamine molecules by running QM/MM trajectories for 10 ps at constant temperature (300 K) and volume in both the S_0 and S_1 electronic states. These trajectories were computed using a 1 fs time step, in combination with the v-rescale thermostat ($\tau_T = 0.1$ ps).[73]

B. Molecular dynamics of cavity-molecule systems

1. Excited-state intramolecular proton transfer in HBQ

After the equilibration at the QM/MM level, HBQ molecules were coupled to a single-mode cavity and two sets of simulations were performed: *(i)* test simulations of two molecular ensembles with $N_{\rm tot} = 6$ and $N_{\rm tot} = 16$ molecules, respectively, and *(ii)* simulations of multiple molecules in a system with variable Rabi splitting. In all simulations, the ESIPT reaction was tracked by measuring the distance between the hydroxyl oxygen and the proton (Figure 2a), and the reaction was considered to have happened if the O-H distance exceeded 0.125 nm.

In the simulations of set *(i)*, the cavity resonance was negatively detuned by 50 meV with respect to the first excited state of HBQ, which is 4.08 eV at the TDA-DFT/CAM-B3LYP//6-31G(d) level of theory. With a cavity field strength of 0.00132791 a.u. (6.80 MV/cm) in the simulation of six molecules and of 0.000813175 a.u. (4.16 MV/cm) in the simulation of 16 molecules, the Rabi splitting was $\sim$240 meV in both simulations. To estimate the validity of the supermolecule approach, we first performed simulations with all molecules in the two ensembles treated as normal molecules (*i.e.*, $N = N_{\rm tot}$), and then replaced four molecules by a single supermolecule in the ensemble of six molecules (*i.e.*, $N_{\rm tot} = 6$, $N = 2$, $N_{\rm S} = 1$, and $M = 4$), and eight molecules by two supermolecules, each representing four normal molecules, in the ensemble of 16 molecules (*i.e.*, $N_{\rm tot} = 16$, $N = 8$, $N_{\rm S} = 2$, and $M = 4$). In both cases, the starting configurations of all molecules were identical, and the system was instantly excited into the lower polariton. The initial velocities were selected randomly from a Maxwell-Boltzmann distribution at 300 K and were the same in the simulations with and without supermolecules.

In the simulations of set *(ii)*, the cavity mode was tuned to be resonant with the first excited electronic state of HBQ (4.08 eV), and had a decay rate of 100 ps^{-1}. With a cavity vacuum field strength of 0.00013859 a.u. (0.71 MV/cm), the Rabi splitting was 100 meV for a system with 100 normal HBQ molecules. We then replaced five normal molecules by five supermolecules (*i.e.*, $N = 95$ and $N_{\rm S} = 5$) and varied the total number of molecules, $N_{\rm tot}$, by changing the number of molecules, M, each of these supermolecules represents (Table I). The values for M were chosen to gradually increase the Rabi splitting at the start of the simulation, when all molecules have the same geometry, from 100 meV to 500 meV in steps of 50 meV. Thus, in these simulations, the number of normal molecules plus supermolecules remained constant (*i.e.*, $N + N_{\rm S} = 100$), whilst the effective number of total molecules increased (*i.e.*, $N_{\rm tot} = N + MN_{\rm S}$). All simulations were started in the optically accessible LP state, with the same initial coordinates and velocities, taken from a Maxwell-Boltzmann distribution at 300 K.

TABLE I. Coarse-grained simulation setups for HBQ molecules coupled to a single-mode cavity with $\hbar\omega_{\rm cav} = 4.08$ eV and $|\mathbf{E}| = 0.71$ MVcm^{-1}, for various total numbers of molecules ($N_{\rm tot}$, first column), "normal" molecules (N, second column), and supermolecules ($N_{\rm S}$, third column), each of which combines a different number, M, of molecules (fourth column). The fifth column lists the Rabi splittings at the start of the simulation ($\hbar\Omega_{\rm R}$).

$N^{\rm tot}$	N	$N_{\rm S}$	M	$\hbar\Omega_{\rm R}$, meV
100	100	0	–	100
225	95	5	26	150
400	95	5	61	200
625	95	5	106	250
900	95	5	161	300
1225	95	5	226	350
1600	95	5	301	400
2025	95	5	386	450
2500	95	5	481	500

2. Population dynamics of Rhodamine-cavity system

The Rhodamine-cavity system was modelled by placing multiple Rhodamine molecules, including water, in a lossless single-mode cavity. Two sets of simulations were performed: *(i)* simulations of polariton relaxation after instantaneous excitation into the UP state for different vacuum field strengths, and *(ii)* short-time simulations of the population relaxation from dark states into lower polaritonic states for different numbers of molecules in the cavity. For tracking the population dynamics, we distinguished between bright lower (LP) and upper polaritonic states (UP) on the one hand, and the dark states (DS) on the other hand, based on a numerical threshold of 0.03 for the contribution of the cavity mode to a polaritonic state $|\psi^m\rangle$. Thus, states with $|\alpha^m|^2 \geq 0.03$ were considered bright, whereas states with $|\alpha^m|^2 < 0.03$ were considered dark.

In the simulations of set *(i)*, the cavity was red-detuned by 170 meV with respect to the excitation energy of Rhodamine (4.18 eV at the CIS/3-21G//Amber03 level of theory). A total number of $N_{\rm tot}$ = 3664 molecules was coupled to the cavity. Of these molecules, $N = 64$ were normal while the remaining 3600 molecules were coarse-grained into $N_{\rm S} = 36$ supermolecules, representing $M = 100$ molecules each. The starting geometries of the molecules were the same. Starting velocities for the atoms in each of the molecules were randomly selected from a Maxwell-Boltzmann distribution at 300 K, and kept the same for the different simulations in this set. The effect of the cavity vacuum field on the molecular dynamics of the normal molecules and on the population dynamics of the total molecule-cavity system was explored by scaling down the absolute value of the vacuum field acting on the normal

molecules with a factor f, while keeping the Rabi splitting at the start of the simulations constant at 308 meV through scaling the vacuum field that acted on the supermolecules by a factor $P = \frac{f^2 N_{\mathrm{tot}} - N}{N_S M}$ (Table II). The simulations were initiated in the UP state, which could be easily identified at the start of the simulation, when there are only two bright states, as all molecules still have the same excitation energy.

TABLE II. Parameters of simulations of the population dynamics in the Rhodamine-cavity system with various vacuum field strengths $|\mathbf{E}_{\mathrm{norm}}|$ at the position of the 60 normal molecules (first and second columns). To have the same Rabi splitting of 308 meV in all simulations, the vacuum field strength $|\mathbf{E}_S|$ at the position of the 100 supermolecules was scaled by factor of P (third column), which compensates for the modification of the interaction strength of normal molecules with the cavity modes.

$\lvert\mathbf{E}_{\mathrm{norm}}\rvert$, a.u.	$\lvert\mathbf{E}_{\mathrm{norm}}\rvert$, MV/cm	scaling factor P
0.000875	4.48	0.003
0.000125	0.64	1.00
0.000063	0.32	4.05
0.000031	0.16	16.27
0.000016	0.08	65.12
0.000008	0.04	260.53

In the simulations of set *(ii)*, the cavity mode energy was resonant with the first electronic excited state (S_1) of Rhodamine. To investigate how the density of dark states influences the relaxation of population from DS manifold into the LP, we varied the total number of molecules, which determines the number of dark states, while keeping the Rabi splitting the same at 100 meV by adjusting the cavity electric field strength (Table III). The total number of molecules was modelled by 60 normal and four supermolecules except for simulations with 16 and 64 molecules, in which all molecules were normal.

Experimentally, the dark states in a cavity are typically excited indirectly by pumping a higher-energy electronic transition in a molecule.[32,74–78] Theory,[79,80] and simulations[41,81–84] suggest that the excited molecule then relaxes into a local minimum on the S_1 potential energy surface prior to population transfer into other polaritonic states. The ensembles were therefore prepared with one of the normal molecules, j, in the S_1 geometry, which was extracted from a S_1 QM/MM MD trajectory, while using the same initial S_0 configuration, extracted from the S_0 QM/MM MD trajectory, for all other molecules. The simulations were started in the lowest energy dark state (DS_0), in which the excitation is localized on the molecule, j, in the S_1 geometry (*i.e.*, $|\beta_j^{\mathrm{DS}_0}|^2 = 0.999$). Because the Stokes shift of our Rhodamine model is 210 meV, this dark state is 0.160 meV lower in energy than the LP.

3. Polariton transport

To model polariton-mediated exciton transport, we placed 640 Rhodamine molecules, 512 of which were normal and 128 were supermolecules, on the z-axis of a periodic one-dimensional Fabry-Pérot microcavity.[35,38] As in previous simulations.[39,85] the cavity dispersion, $\omega_{\mathrm{cav}}(k_{z,p}) = \sqrt{\omega_0^2 + c^2 k_{z,p}^2}$, was modelled with 160 discrete modes (*i.e.*, $k_{z,p} = 2\pi p/L_z$ with $0 \le p < 160$ and $L_z = 50$ μm). The cavity resonance was red-detuned by 370 meV with respect to the Rhodamine absorption maximum at the CIS/3-21G//Amber03 level of theory (4.18 eV), corresponding to a distance of $L_x = 0.163$ μm between the mirrors. To keep the polariton dispersions for the cavities containing both normal molecules and supermolecules, the same as for a cavity with only normal molecules, the molecules were placed on the z-axes of the cavity as follows:[47] The normal molecules were positioned in one half of the box, with intermolecular spacings of $\Delta z_{\mathrm{norm}} = L_z/N_{\mathrm{tot}}$. The supermolecules in the other half of the cavity were separated by $\Delta z_S = M(L_z/N_{\mathrm{tot}})$. The distance between the last normal molecule and the first supermolecule at the boundary between the normal and supermolecules was $\Delta z_{\mathrm{edge}} = (\Delta z_{\mathrm{norm}} + \Delta z_S)/2$. With a cavity vacuum field strength of 0.00005 au (0.26 MV/cm) and a total number of molecules of 768 ($M = 2$), 1024 ($M = 4$), and 1280 ($M = 6$), the Rabi splitting was 282 meV, 325 meV, and 363 meV, respectively.

TABLE III. Parameters for simulations of relaxation from dark into bright polaritonic states in Rhodamine cavities. The first two columns list the vacuum field strength $|\mathbf{E}|$ in atomic and SI units. The third column lists the total number of molecules N_{tot} coupled to the cavity. The fourth column lists the number of molecules that are grouped together into a single supermolecule, such that with four such supermolecules and 60 normal molecules, the total number of molecules in the simulation is $N^{\mathrm{tot}} = 60 + 4M$.

$\lvert\mathbf{E}\rvert$, a.u.	$\lvert\mathbf{E}\rvert$, MV/cm	N_{tot}	M
0.000129548	0.663	16	–
0.000064774	0.332	64	–
0.000032387	0.166	256	49
0.000016194	0.083	1024	241
0.000008097	0.041	4096	1009
0.000004048	0.021	16384	4081
0.000002024	0.010	65536	16369
0.000001012	0.005	262144	65521

As before,[39] polariton transport was initiated both resonantly and off-resonantly. In the resonant excitation scheme, a Gaussian wavepacket of lower polaritons centred at $z = 5$ μm in real space and at $k_z = 6.91$ $\mu\mathrm{m}^{-1}$ in reciprocal space with a width of 0.707 $\mu\mathrm{m}^{-1}$, was created.[86] For off-resonant excitation, simulations were started in the S_1 electronic excited state of a single (normal) molecule that was located at $z = 5$ μm.

The propagation of the polariton wavepacket was monitored as the probability amplitude of the total wave function (Equation 20), calculated as the sum of the excitonic component

$$|\Psi_{\mathrm{exc}}(z_j,t)|^2 = |d_j(t)|^2, \tag{21}$$

with $1 \le j \le N + N_S$, and the photonic component, which was Fourier transformed into real space first

$$\begin{aligned} |\Psi_{\mathrm{phot}}(z_j,t)|^2 &= \left[\mathcal{FT}^{-1} \textstyle\sum_p^{n_{\mathrm{modes}}} d_p(t)\right]^2 = \\ &\left[c_{\mathrm{norm,super}} \textstyle\sum_p^{n_{\mathrm{modes}}} d_p(t) e^{ik_{z,p} z_j}\right]^2, \end{aligned} \tag{22}$$

with $N+N_S \leq p \leq N+N_S+n_{\text{modes}}$ and coefficients $c_{\text{norm}} = \sqrt{1/N_{\text{tot}}}$ and $c_{\text{super}} = \sqrt{M/N_S}$ that correspond to the coordinates of normal and supermolecules, respectively, and are used to normalize the wavepacket (SI, section 1.3). The propagation distance was analysed by calculating the mean square displacement (MSD) of the total polariton wavepacket $|\Psi(z,t)|^2$:

$$\text{MSD} = \frac{\langle\Psi(z,t)|(\hat{z}(t)-\hat{z}(0))^2|\Psi(z,t)\rangle}{\langle\Psi(z,t)|\Psi(z,t)\rangle} \tag{23}$$

with $\hat{z}(t)$ the position operator at time t.

IV. RESULTS AND DISCUSSION

To find out if the proposed hybrid normal molecules / coarse-grained supermolecules ansatz can provide further insights into the dynamics of exciton-polaritons, we performed molecular dynamics simulations in which we systematically investigated the interplay between cavity mode volume (or, equivalently, the vacuum field strength) on the one hand, and the total number of collectively-coupled molecules (*i.e.*, normal plus supermolecules) on the other hand, for (A) ultrafast photochemistry, (B) polariton relaxation and (C) exciton transport in cavities.

A. Excited-state intra-molecular proton transfer

Upon photo-excitation, bare HBQ molecules undergo an excited-state intra-molecular proton transfer (ESIPT) reaction within several tens of femtoseconds.[87–91] Because this timescale is comparable to the cavity lifetimes attained in typical experiments on strong coupling with organic molecules,[32,92,93] the ESIPT in HBQ has been employed in recent work as a model reaction for exploring the effects of strong light-matter coupling on photochemistry.[13]

1. Consistency between simulations with normal molecules only and simulations with both normal and supermolecules

To verify that the dynamics of N_{tot} HBQ molecules remains consistent after grouping together N_S batches of M molecules into N_S supermolecules, we performed simulations with both $N = N_{\text{tot}}$ normal molecules and $N+N_S M = N_{\text{tot}}$ supermolecules, and compared the time of proton transfer after excitation into the lower polariton.

When all molecules were normal, excitation into the LP state of both the $N_{\text{tot}} = 6$ and $N_{\text{tot}} = 16$ molecule systems was followed by an ESIPT reaction in one of the HBQ molecules, as indicated by a substantial increase of the distance between the donor (oxygen) and proton (hydrogen) atoms in that molecule (figure 2**a**). In the other molecules this distance did not increase and the proton remained bound to the oxygen (figure 3**a** and **c**). When eight molecules of the ensemble were grouped into two supermolecules each representing four normal molecules, the outcome remained essentially unaltered in the ensemble of 16 molecules, with the same normal molecule undergoing the ESIPT reaction (red lines in figure 3**c** and **d**).

However, in the ensemble of six molecules, grouping four molecules into a supermolecule delayed the ESIPT reaction by about twenty femtoseconds (red lines in figure 3**a** and **b**). This discrepancy stems from a difference in the contributions of the M normal molecules to the Hellman-Feynman gradients associated with atoms of those molecules (equations 18 and 19) when these molecules are normal as compared to when these molecules are coarse-grained into a supermolecule. In the former situation, the M normal molecules evolved *independently* during the dynamics, and therefore, the expansion coefficients associated with these molecules, evolved differently, *i.e.*, $|\beta_i^k|^2 \neq |\beta_{j\neq i}^k|^2$. In contrast, because the dynamics of these molecules are constrained to evolve in the same way when coarse-grained into a supermolecule, their expansion coefficients are forced to remain the same, *i.e.*, $|(\beta_S^k)_i|^2 = M|\beta_i^k|^2$. Accordingly, the Hellman-Feynman gradients and hence the forces acting on the atoms in all molecules, were different in simulations *i)* and *ii)* with the discrepancy accumulating over time and eventually resulting in a different reaction time in the ensemble of six molecules.

As we show in the Supporting Information, the same (within numerical error) dynamics can be achieved if we assign identical starting coordinates *and* velocities to each of M normal molecules, and use the same coordinates and velocities for the supermolecule as well (figures S1 and S3). Nevertheless, despite this small discrepancy for the smaller ensemble of six molecules, coarse-graining provides a consistent description of the molecular dynamics under strong coupling conditions, as the same normal molecule underwent the ESIPT reaction in both cases.

We emphasize that because the dynamics of the molecules forming a supermolecule are identical, supermolecules cannot react within the single-excitation subspace of the Tavis-Cummings model. While it has been suggested that under very specific circumstances, a single photon could trigger multiple reactions sequentially,[94] a reaction of a supermolecule describes a concerted reactivity in M molecules,[95] and would thus require the absorption of M photons instead. Indeed, as shown in figure 3**b** and **d**, the supermolecules did not undergo ESIPT, and, as we show in the SI, there were no reactions at all when the normal molecules were frozen and only the supermolecules were allowed to move (figure S2).

2. The effect of the molecular concentration on the ESIPT reaction rate

The rate of the proton transfer reaction in a cavity depends on how rapidly the excitation transfers from the initially excited lower polariton into the dark states, in which the excitation is predominantly localized on a single molecule that can subsequently undergo the reaction.[13] Because the rate of this non-adiabatic population transfer process is inversely proportional to the energy difference between the states,[41,76,96,97] the rate can be controlled by varying the Rabi splitting through the HBQ concentration (Equation 4). To investigate how via

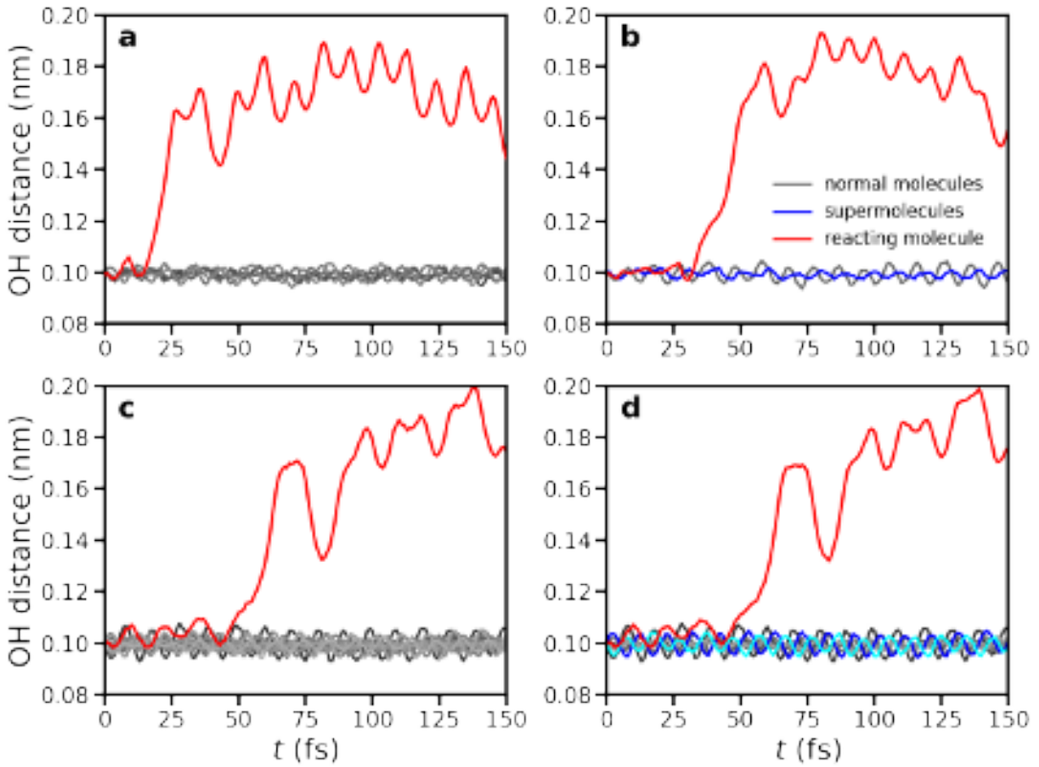

FIG. 3. **Top panels**: Distance between oxygen and hydrogen atoms in HBQ molecules during the dynamics of the system (**a**) with six normal molecules and (**b**) with two normal and a single supermolecule ($M = 4$), such that the total number of molecules remains six, although only three had to be simulated. **Bottom panels**: Distance between oxygen and hydrogen atoms in HBQ molecules during the dynamics of the system with (**c**) 16 normal molecules and with (**d**) eight normal and two supermolecules ($M = 4$), *i.e.*, still 16 molecules in total, but only 10 were simulated. In both cases, the molecules are coupled to a single cavity mode and the LP state is initially excited. The OH distance in normal and supermolecules is shown in shades of grey and blue, respectively, while the distance in the reacting molecule is plotted in red.

the Rabi splitting, the number of molecules affects the ESIPT rate after excitation into the LP, we performed simulations of $N = 95$ normal molecules plus $N_S = 5$ supermolecules, and systematically varied the total number, N_{tot}, of molecules that are coupled to a single cavity mode by grouping different numbers of molecules, M, into the supermolecules (Table I).

In Figure 4 we show that upon increasing the number of HBQ molecules, and concomitantly the Rabi splitting, the rate of ESIPT decreased, as the reaction time went up. This trend is roughly anti-correlated with the spectral overlap between the LP and the HBQ absorption, which is plotted in purple and also visualised in Figure S4. This observation is in line with previous findings,[56,98] which suggest that rate at which population transfers from the initially excited LP into the dark state manifold is proportional to the overlap.

At higher Rabi splitting, the LP overlaps with states that belong to molecular configurations with lower excitation energies. To rule out that such configurations may have a lower reaction rate, and that, therefore, the reduction in reaction rate when increasing the Rabi splitting, could be due to the population transferring from the LP into these states, we performed 500 excited-state QM/MM simulations of HBQ without cavity and correlated the reaction time with the S_1-S_0 energy gap at the start of the simulation (Figure S5). While a linear regression to the data points suggests a tiny reduction in rate with increasing excitation energy, the correlation is very weak, and furthermore opposite to the trend observed in Figure 4. Thus, the reduction of the rate with increasing Rabi splitting cannot be attributed to differences in reaction rates of the molecular configurations.

B. Population dynamics of Rhodamine-cavity systems

1. *Population dynamics in a cavity with realistic vacuum field*

Because modifying the mode volume of a Fabry-Pérot cavity by changing the distance between the mirrors compromises the resonance conditions (unless a higher order cavity mode becomes resonant again, as was done in Bhuyan *et al.*[99]), the Rabi splitting is normally controlled by varying the number of molecules within the mode volume (Equation 4). However, due to restrictions on hard- and software, increasing the number of molecules in simulations is challenging, which has of-

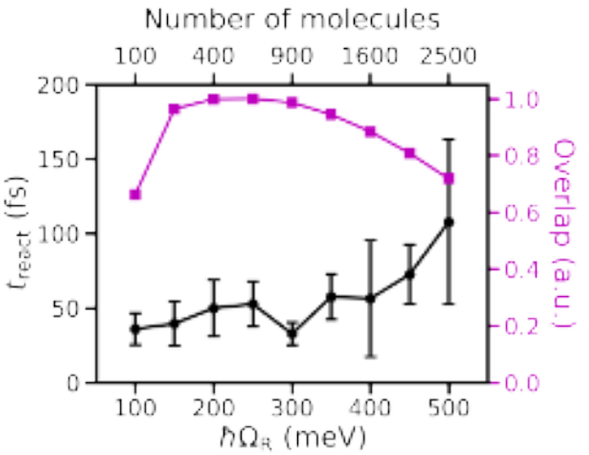

FIG. 4. Reaction time of the proton transfer of a single HBQ molecule in an ensemble of HBQ molecules strongly coupled to a single-mode cavity (black circles) and the normalized overlap integral between dark and bright polaritonic states (purple squares) as a function of the Rabi splitting, $\hbar\Omega_R$. The plotted values are averages of five simulations, and error bars are the associated standard deviations. Parameters of the simulations are provided in Table I.

ten prompted computational chemists to increase the strength of the vacuum field instead. Indeed, by applying vacuum fields that are orders of magnitude higher than in experiments, strong coupling can even be achieved with single molecules in simulations. While such high fields have been shown to induce significant changes to the dynamics and reactivity, it is not *a priori* clear how to translate these insights to experiments and provide a rationale for the changes observed in the latter.

To explore the influence of the cavity vacuum field strength on the molecular dynamics of molecules in the collective strong coupling regime, while keeping both the Rabi splitting and the total number of molecules unaltered, we separately scaled the vacuum field for the normal molecules and for the supermolecules. By focusing on the normal molecules, we systematically investigated the effect of strong coupling on the local dynamics when the vacuum field acting on these normal molecules approaches the low values of experiments. To compensate for the decrease in the collective light-matter coupling when the vacuum field at the normal molecules is scaled down, we simultaneously scaled up the interaction of the supermolecules with the vacuum field by a factor P. Because the Rabi splitting is proportional to the electric field strength E_{cav} and the total number of molecules, *i.e.*, $\hbar\Omega_R \sim E_{cav}\sqrt{N_{tot}} = E_{cav}\sqrt{N+N_S M}$, a reduction of the vacuum field acting on the normal molecules by a factor of f is thus compensated by an increase of the vacuum field for the supermolecules by $(E_{cav}/f)\cdot f\sqrt{N+N_S M} = (E_{cav}/f)\cdot\sqrt{N+N_S MP}$, such that $P = \frac{f^2 N_{tot}-N}{N_S M}$ (Table II).

We performed simulations of in total 3664 Rhodamine molecules treated as 64 normal molecules and 36 supermolecules, each representing 100 identical molecules (*i.e.*, $N_{tot} = 3664$, $N = 64$, $N_S = 36$ and $M = 100$). The frequency of the cavity mode was red-detuned by 174 meV with respect to the first-excited state of Rhodamine. In all simulations, the Rabi splitting was $\hbar\Omega_R = 308$ meV.

In figure Figure 5**a** we show that after instantaneous excitation into the upper polariton, population quickly transferred into the dense manifold of dark states, reaching more than 80% after 100 fs of simulation, in line with theoretical predictions.[79,80] The rest of the population remained distributed between the upper and lower polaritonic states (Figure 5**a**). This trend in ultra-fast relaxation from the UP into the dark states was observed for the complete range of electric field strengths per normal molecule (0.04-0.64 MVcm^{-1}, Figure 5**b**).

We note that at the start of the simulation, the population oscillates between the UP and DS with a period of approximately 10 fs. Although this timescale is close to the Rabi period of 13 fs, we emphasize that the population cannot undergo Rabi oscillations, as the simulations were started in an adiabatic eigenstate of the molecule-cavity system (*i.e.*, the UP). Instead, we attribute this oscillation to a high-frequency molecular vibration, which has a displacement that overlaps with the non-adiabatic coupling vector connecting the UP to the dark state manifold (Figure S6),[41] and a period of 9.8 fs (3395.4 cm^{-1}) that closely matches the oscillation in the populations (Figure 5**a**).

For all cavity fields, the molecular dynamics of the normal molecules were nearly identical (Figure S7a), suggesting that the cavity field strengths employed here had no major influence on the structure and dynamics of the molecules. While for the smaller vacuum field strengths, the population dynamics were also nearly identical (Table S1), upon increasing the field strength, small deviations in the population dynamics become visible in Figure 5**b**, which are corroborated by a comparison of the correlation coefficients between these plots (Table S1).

To further explore how a larger vacuum field strength affects the collective polariton dynamics, we performed an additional simulation with the electric field of 4.48 MVcm^{-1}, which is comparable to the fields used in theoretical studies on a single-molecule strong coupling.[43,48,84,100,101] In our trajectories, such extremely large cavity field strength caused a deviation of the population dynamics with respect to the simulations with the weaker vacuum fields, which would be required to achieve strong coupling with a macroscopic ($\sim 10^6$) number of molecules (Figure 5**c** and Table S1). While the trends were qualitatively similar, as at all field strengths, 80% of the population had transferred from the UP into the dark state manifold within 100 fs, the quantitative differences suggest that care should be taken when generalising the results obtained with single-molecule simulations to the case of experimentally meaningful ensemble sizes.[43] Nevertheless, also at the largest vacuum field, the local dynamics of the normal Rhodamine molecules was similar to that at the weaker field strengths (Figure S7b), which we attribute to the fact that even for the largest field, the forces due to the coupling with the field are still much smaller than the other forces acting on the molecules.

Finally, we repeated the simulations for $N_{tot} = 256$ Rho-

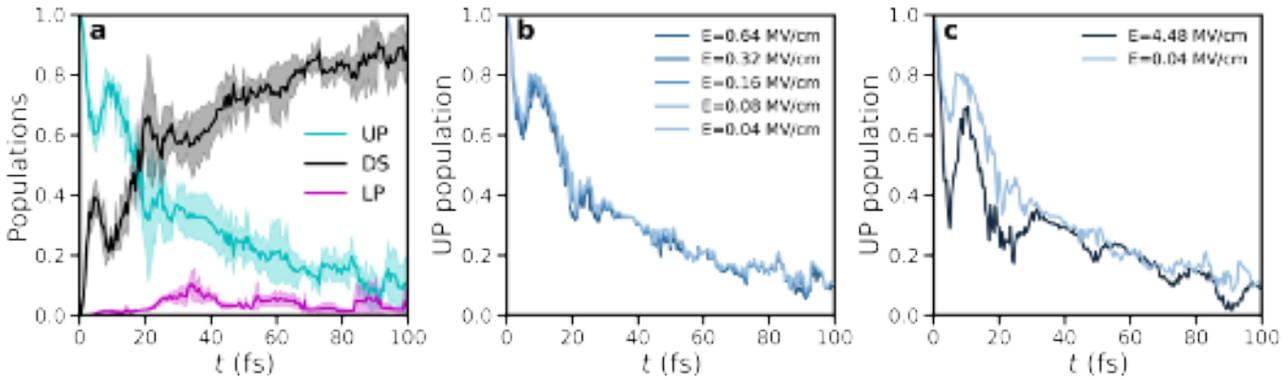

FIG. 5. Population dynamics of the Rhodamine-cavity system for different cavity vacuum fields acting on the 64 normal molecules. (**a**) Population dynamics of the upper polariton (UP), lower polariton (LP), and dark states (DS) in a cavity with a vacuum field strength of 0.64 MV/cm (0.000125 a.u.). The solid lines represent averages of four simulations, while the shaded areas represent the standard deviation. (**b**) Time-resolved populations of the UP in cavities with vacuum field strengths that act on the normal molecules, ranging from 0.04 MV/cm (0.000008 a.u.) to 0.64 MV/cm (0.000125 a.u.). Panel (**c**) Population dynamics of the UP in cavities with an electric field required for single-molecule strong coupling ($E = 4.48$ MVcm^{-1}, or 0.000875 a.u.) and for strong coupling with a macroscopic number of molecules ($E = 0.04$ MV/cm, or 0.000008 a.u.).

damine molecules to investigate how the size of the supermolecules affects the population dynamics. As shown in Figure S8, varying M and N_S under constant Rabi splitting (300 meV), leads to small variations in the population dynamics that are comparable to the variations due to thermal disorder in simulations without supermolecules. As explained in the SI, we attribute these variations to differences in the nonadiabatic coupling due to changes in the molecular displacements that occur when simulations are started with different initial velocities, or when molecules are grouped into supermolecules.

2. *Population transfer between dark and bright states*

Understanding polariton relaxation is crucial for exploiting polaritons in optical devices, such as light emitting diodes,[102] or lasers.[103] For both types of application, transfer from dark into bright states is the key to an efficient outcoupling of light. In particular, for polaritonic lasing this relaxation process needs to be sufficiently efficient to compete with cavity losses and build up a macroscopic population in the lowest energy polaritonic state for stimulating Bose-Einstein condensation.[104] The rate of this relaxation depends on the number of molecules and was found to scale as $1/N_{\text{tot}}$.[33,34,84,99,105]

Previously, we could demonstrate with MD simulations that this $1/N_{\text{tot}}$ scaling holds for molecular ensembles of up to a few hundred molecules at constant Rabi splitting.[41] Here, we extend the analysis to verify if this trend is maintained also when the number of molecules approaches the experimentally relevant limit, where entropy favors population of the dark state manifold.[106] As before, we initiated the trajectories with one of the (normal) molecules in the relaxed S_1 state and monitored the build-up of the cavity mode population during the first 1 fs of the simulation. We gradually increased the total number of molecules (N_{tot}), while keeping the Rabi splitting at 100 meV by scaling down the vacuum field strength (Table III). Because 1 fs is too short for thermal motions to significantly broaden the distribution of the molecular excitation energies, we could clearly distinguish the dark states, which have a negligible cavity mode contribution, from the bright polaritonic states, which have a cavity mode contribution of nearly 50%, and track the population transfer into LP state directly by monitoring the evolution of the population in the cavity mode.

In Figure 6**a**,**b** we plot the evolution of the cavity mode contribution to the polaritonic states for ensemble sizes from 16 to 262144 molecules. These plots suggest that population transfer rate decreases when the number of molecules is increased. To quantify this observation we used first-order time-dependent perturbation theory, which predicts that the initial population dynamics follows the Rabi formula:

$$|c_{\text{LP}}(t)|^2 = \frac{4|V_{\text{DS,LP}}|^2}{\omega_{\text{DS,LP}}^2+4|V_{\text{DS,LP}}|^2}\times \sin^2\tfrac{1}{2}\left(\sqrt{\omega_{\text{DS,LP}}^2+4|V_{\text{DS,LP}}|^2}\right)t, \tag{24}$$

where $|c_{\text{LP}}(t)|^2$ is the population in the LP state, $\hbar\omega_{\text{DS,LP}}$ is the energy gap between DS and the LP. Because the population transfer between polaritonic states is driven by the nonadiabatic, or vibronic coupling, which determines the mixing of the states due to molecular motions,[107–109] the perturbation term $V_{\text{DS,LP}}$ represents this nonadiabatic coupling and is determined as[110]

$$V_{\text{DS,LP}} = \mathbf{d}_{\text{DS,LP}} \cdot \dot{\mathbf{R}}. \tag{25}$$

In this expression, $\dot{\mathbf{R}}$ is a vector containing the velocities of all atoms in the system and $\mathbf{d}_{\text{DS,LP}}$ is the non-adiabatic coupling

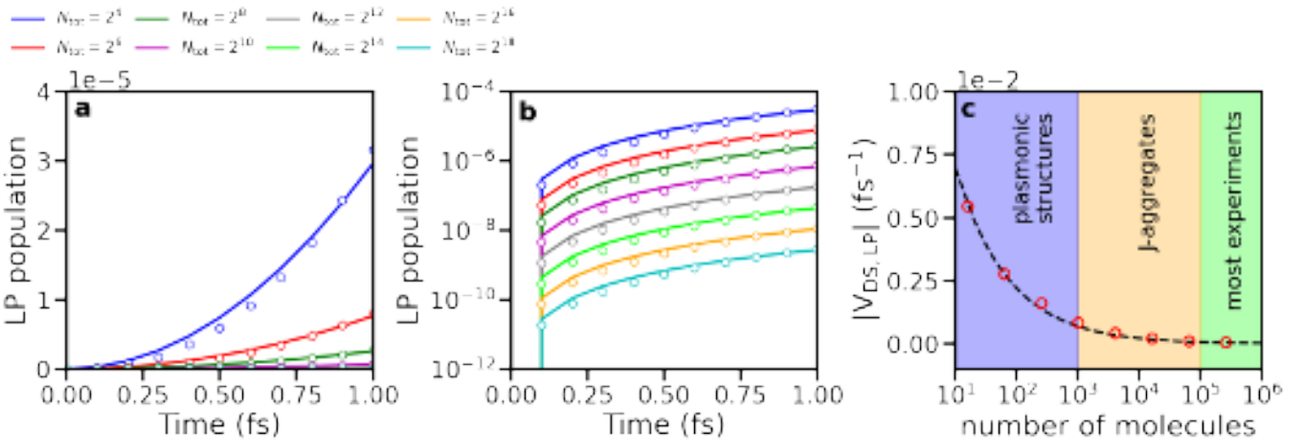

FIG. 6. Population relaxation rate from a dark state to the LP state as a function of time and number of molecules. Panels **a** and **b**: Cavity mode's population during the first one femtosecond of simulation plotted in linear (**a**) and logarithmic (**b**) scale. The number of molecules N_{tot} ranges from 2^4 to 2^{18}. Circles show the simulation data points, and solid lines are fits to the Rabi formula (Equation 24). Panel **c**: Absolute value of the perturbation term $|V_{\text{DS,LP}}|$, obtained from the fits in panel **a**, for various N_{tot}. Open circles are data points, and the continuous line is a fit to $a/\sqrt{N_{\text{tot}}}$ with $a = 0.022$ fs^{-1}. Blue, yellow and green areas indicate the ranges of N_{tot} that are relevant for different kinds of experiments.

vector:

$$\mathbf{d}_{\text{DS,LP}} = \frac{\langle \psi^{\text{LP}} | \nabla_{\mathbf{R}} \hat{H} | \psi^{\text{DS}} \rangle}{E_{\text{DS}} - E_{\text{LP}}} \tag{26}$$

The direction of this vector defines in what direction population is transferred between the polaritonic states, while its magnitude determines how much population is transferred.

Using the Rabi formula, we fitted the time-evolution of the cavity mode population (solid lines in figure 6**a**,**b**) to estimate the values of $|V_{\text{DS,LP}}|$ for different ensemble sizes and plot these values in figure 6**c**. The non-adiabatic couplings in this plot scale as $1/\sqrt{N_{\text{tot}}}$, confirming that also for larger N_{tot}, the initial rate of population transfer from the DS into LP scales as $1/N_{\text{tot}}$, in line with our previous predictions for smaller N_{tot}.[41]

Two mechanism have been proposed for population transfer from the dark state manifold into the lower polariton: vibrationally assisted scattering (VAS),[76,78–80] and radiative pumping (RP).[96,111] In VAS, transitions between the dark states and bright light-matter states are accompanied by discrete changes in the eigenstates of specific molecular vibrations, whereas in RP, the fluorescence from an uncoupled molecule excites a polariton. By deriving analytical rate expressions for VAS and RP, Pérez-Sánchez and Yuen-Zhou have recently demonstrated that the aforementioned vibrational resonance conditions coexist for both mechanisms,[112] making it difficult to identify which mechanism operates in our simulations. However, because they also found that the RP contribution to the relaxation process scales as $(N-1)/N^2 \approx 1/N$, whereas VAS scales as $1/N^2$,[112] we speculate that radiative pumping dominates the relaxation process in our simulations.

From the plot in figure 6**c**, we can estimate the rate of the polariton emission in realistic molecule-cavity systems. Under the assumption that the lifetime of the lower polariton is determined by the cavity lifetime,[56,79,80] and that the latter is short compared to $1/|V_{\text{DS,LP}}|$, population transferred into the LP state is immediately lost due to emission. Therefore, the value of the non-adiabatic coupling provides a rough estimate for the emission rate constant. In most experiments, the number of strongly-coupled molecules is believed to be on the order of 10^5-10^8 molecules per cavity mode[33,34,52,53] (green area in Figure 6**c**). For this range, we can anticipate emission on a pico- to nanosecond timescale, which is in line with experimental observations.[92,96,111] In contrast, for molecular ensembles of up to thousand molecules, we predict emission on an ultra-fast femto- to picosecond timescale, which could potentially be achieved with plasmonic nanosctructures[113,114] (blue area in figure 6**c**).

A special case are J-aggregates of molecular dyes. Due to supramolecular self-organisation of individual molecules into agglomerates, J-aggregates have an enhanced transition dipole moment, which makes them an excellent platform for achieving strong coupling. Recent experiments suggest that the concentration of excitons in J-aggregates of 5,5',6,6'-tetrachloro-1,1'-diethyl-3,3'-di(4-sulfobutyl)-benzimidazolocarbocyanine (TDBC) dyes could be on the order of 10^{17} cm^{-3}.[115] Assuming that for a Fabry-Pérot cavity, the cavity mode volume is proportional to the cube of the wavelength, $V \sim \lambda^3$,[116] and that the cavity is at resonance with the absorption maximum of a J-aggregate at $\sim$2 eV,[32,115,117] the number of excitons in this volume would be on the order of $\sim 10^5$. Considering furthermore that strong light-matter coupling may significantly enhance the exciton coherence length in J-aggregates,[118] the number of excitons in a cavity could be even smaller (yellow area in figure 6**c**), for which we would estimate an emission on a (sub) picosecond timescale. Indeed, time-resolved spectroscopy measurements have demonstrated polariton emission on such ultrashort timescales for a J-aggregate-cavity system.[78]

C. Polariton transport

We simulated polariton transport in a one-dimensional chain of Rhodamine molecules collectively coupled to a multi-mode Fabry-Pérot cavity both after *i)* resonant excitation of a Gaussian wavepacket of the lower polariton states, and after *ii)* off-resonance excitation into the first excited state of a single molecule. The Rabi splitting was varied between 282 meV and 363 meV by changing the total number of molecules, N_{tot}, while keeping the number of normal and supermolecules the same, as described in the Simulation details section.

Figure 7**a**-**c** shows the time-space propagation plots of the polariton wavepackets after resonant excitation, and in figure 7**d** the mean squared displacement (MSD) of these wavepackets is plotted. In all simulations, the transport underwent a transition from a ballistic into a diffusion regime around 75 fs, as evidenced by a change from a quadratic to a linear dependence of the MSD at that time point. As was suggested previously,[39,119] this transition is due to reversible population transfer between the LP states with group velocity, and the immobile dark states, which eventually causes the initially ballistic wave packet to move in a diffusive manner. For the three different Rabi splittings the MSDs are very similar during the 200 fs of the simulation. This similarity suggests that within the range of Rabi splittings tested here, there is sufficient overlap between LP and DSs to mediate the fast transition from the initial ballistic into the diffusion regime. For larger Rabi splittings, when the overlap is smaller or even absent, we anticipate a longer duration of the ballistic phase. However, because in lossy cavities, such prolonged ballistic motion is accompanied by an enhanced decay into the ground state, the distance over which the polaritons can move ballistically would be limited.[85,120]

A different picture was observed after off-resonant excitation, for which the transport of the wavepackets is visualized in figure 7**e**-**g**. After a short relaxation period, characterized by the initial slowdown of the wavepackets due to destructive interference,[121] the propagation proceeded as a diffusion process, as manifested by a linear growth of the MSD in figure 7**h**. The propagation velocity decreased with increasing Rabi splitting, which we attribute to a slower relaxation of the population into the LP branch, as the non-adiabatic coupling that drives this relaxation, is inversely proportional to both the energy gap between the states (Equation 26) and the number of molecules (Figure 6**c**).[41] As a result, the cavity mode population of the polariton wavefunction was highest for the smallest Rabi splitting (Figure S9**b**), which promoted the most efficient transport on a short timescale. It is important to note that this trend differs from the trend obtained for simulations with frozen molecular degrees of freedom, *i.e.*, at the absolute zero temperature, at which the MSD was similar for all three Rabi splittings (Figure S9**c**). This distinction emphasizes the importance of including nuclear dynamics[122,123] and thermal disorder[124,125] in simulations of polariton-mediated exciton transport.

V. CONCLUSION

Over the past two decades, the phenomenon of strong light-matter coupling has been extensively studied from both experimental and theoretical perspectives, but a gap remains between these two perspectives in terms of what systems are being studied. On the one hand, the majority of experiments are performed with Fabry-Pérot microcavities or distributed Bragg reflectors, which couple millions of molecules. On the other hand, computer simulations can only handle small molecular ensembles, which have often been restricted to just a few molecules. With the aim of narrowing down this gap, we have proposed a multi-scale approach for MD simulations of arbitrarily large molecular ensembles, in which we replaced subsets of molecules by the so-called supermolecules that effectively represent the dynamics of multiple identical molecules. With this approach, we systematically investigated the effect of both the vacuum field strength and the number of coupled molecules, on ultra-fast excited state intramolecular proton transfer, polariton relaxation dynamics, and polariton-mediated exciton transport.

While coarse-graining preserves the number of molecules and, hence, the density of states in the dark state manifold, the dynamic and static disorder are reduced, as the molecules that constitute a supermolecule are forced to be the same. To avoid that the reduced disorder affects the dynamics of the whole ensemble, the number of normal plus supermolecules needs to be sufficiently large for the distribution of the density of states to converge. A simple analysis of the molecular density of states for Rhodamine suggests that inclusion of a hundred molecules would suffice (Figure S10), which is straightforward to simulate with modern computational resources. We emphasize that this number refers to the normal *plus* supermolecules, but not their ratio, as a supermolecule samples the same phase-space as a normal molecule. We anticipate that multi-scale simulations, in which the effects of realistic cavity coupling strengths can be probed at the level of a single molecule, may be the key to understand the interplay between local and collective light-matter interactions, and hence pave the way for exploiting strong coupling in devices, such as light sources or photonic catalysts.

ACKNOWLEDGMENTS

We thank Pavel Buslaev and Arkajit Mandal for valuable discussions and suggestions. We also acknowledge the CSC-IT center for scientific computing in Espoo, Finland, for providing very generous computational resources. This work was supported by the Academy of Finland (Grants 323996 and 332743).

DATA AVAILABILITY STATEMENT

The data that support the findings of this study are available from the corresponding author upon reasonable request.

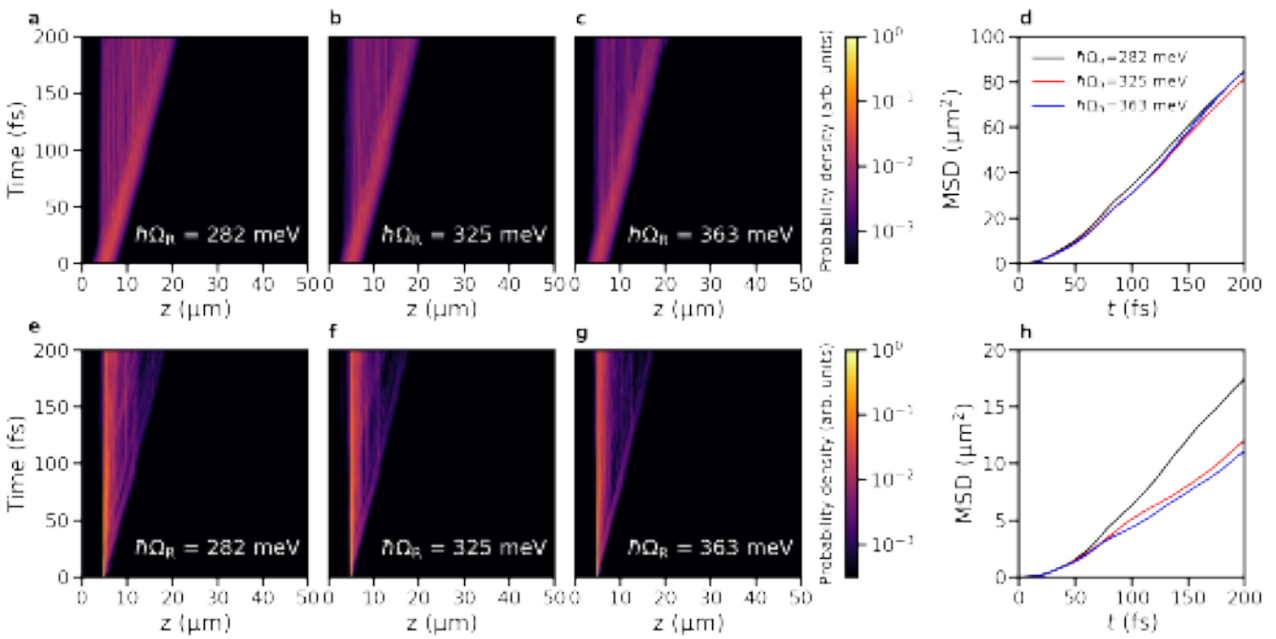

FIG. 7. Polariton propagation after resonant excitation of a wavepacket of LP states (top panels) and off-resonant excitation into a molecule (bottom panels) centred at $z = 5$ μm. The first three columns depict the total probability density $|\Psi(t)|^2$ of the wavepacket in a cavity with the Rabi splitting $\hbar\Omega_R$ of 282 meV (panels **a**, **e**), 325 meV (panels **b**, **f**), and 363 meV (panels **c**, **g**), respectively, as a function of distance (horizontal axis) and time (vertical axis). Panels **d** and **h** show the mean square displacement (MSD, *i.e.*, $\sqrt{\langle(z(t) - \langle z(0)\rangle)^2\rangle}$) of the position of the wavepackets after resonant and off-resonant excitation, respectively. The lines are averages of three simulations.

The code, based on a fork of Gromacs-4.5.3, is available for download at https://github.com/upper-polariton/GMXTC.git

SUPPORTING INFORMATION

The Supporting Information contains derivations of the expectation value of the Tavis-Cummings Hamiltonian and of the Hellman-Feynman gradients in adiabatic and diabatic bases, as well as additional simulations.

[1] J. A. Hutchison, T. Schwartz, C. Genet, E. Devaux, and T. W. Ebbesen, "Modifying chemical landscapes by coupling to vacuum fields," Angew. Chem. Int. Ed. **51**, 1592–1596 (2012).
[2] B. Munkhbat, M. Wersäll, D. G. Baranov, T. J. Antosiewicz, and T. Shegai, "Suppression of photo-oxidation of organic chromophores by strong coupling to plasmonic nanoantennas," Sci. Adv. **4**, eaas9552 (2018).
[3] K. Stranius, M. Herzog, and K. Börjesson, "Selective manipulation of electronically excited states through strong light-matter interactions," Nat. Comm. **9**, 2273 (2018).
[4] A. Thomas, L. Lethuillier-Karl, K. Nagarajan, R. M. A. Vergauwe, J. George, T. Chervy, A. Shalabney, E. Devaux, J. Moran, and T. W. Ebbesen, "Tilting a ground-state reactivity landscape by vibrational strong coupling," Science **363**, 615–619 (2019).
[5] R. M. A. Vergauwe, A. Thomas, K. Nagarajan, A. Shalabney, J. George, T. Chervy, M. Seidel, E. Devaux, V. Torbeev, and T. W. Ebbesen, "Cavity catalysis by cooperative vibrational strong coupling of reactant and solvent molecules," Angew. Chem. Int. Ed. **58**, 15324–15328 (2019).
[6] Y. Yu, S. Mallick, M. Wang, and K. Börjesson, "Barrier-free reverse-intersystem crossing in organic molecules by strong light-matter coupling," Nat Commun **12**, 3255 (2021).
[7] W. Ahn, J. F. Triana, F. Recabal, F. Herrera, and B. S. Simpkins, "Modification of ground-state chemical reactivity via light-matter coherence in infrared cavities," Science **380**, 1165–1168 (2023).
[8] R. F. Ribeiro, L. A. Martinéz-Martinéz, M. Du, J. Campos-Gonzalez-Angule, and J. Yuen-Zhou, "Polariton chemistry: controlling molecular dynamics with optical cavities," Chem. Sci. **9**, 6325–6339 (2018).
[9] M. Hertzog, M. Wang, J. Mony, and K. Börjesson, "Strong light–matter interactions: a new direction within chemistry," Chem. Soc. Rev. **48**, 937–961 (2019).
[10] F. J. Garcia-Vidal, C. Ciuti, and T. W. Ebbesen, "Manipulating matter by strong coupling to vacuum fields," Science **373**, eabd0336 (2021).
[11] I. Vurgaftman, B. S. Simpkins, A. D. Dunkelberger, and J. C. Owrutsky, "Negligible effect of vibrational polaritons on chemical reaction rates via the density of states pathway," The Journal of Physical Chemistry Letters **11**, 3557–3562 (2020).
[12] J. B. Pérez-Sánchez, F. Mellini, N. C. Giebink, and J. Yuen-Zhou, "Collective polaritonic effects on chemical dynamics suppressed by disorder," Phys. Rev. Res. **6**, 013222 (2024).
[13] A. Dutta, V. Tiainen, I. Sokolovskii, L. Duarte, N. Markešević, D. Morozov, H. A. Qureshi, S. Pikker, G. Groenhof, and J. J. Toppari, "Thermal disorder prevents the suppression of ultra-fast photochemistry in the strong light-matter coupling regime," Nat. Commun. **15**, 6600 (2024).
[14] M. V. Imperatore, J. B. Asbury, and N. C. Giebink, "Reproducibility of cavity-enhanced chemical reaction rates in the vibrational strong coupling regime," J. Chem. Phys. **154**, 191103 (2021).
[15] G. D. Wiesehan and W. Xiong, "Negligible rate enhancement from reported cooperative vibrational strong coupling catalysis," J. Chem. Phys. **155**, 241103 (2021).
[16] P. A. Thomas, W. J. Tan, V. G. Kravets, A. N. Grigorenko, and W. L. Barnes, "Non-polaritonic effects in cavity-modified photochemistry," Adv. Mater. **36**, 2309393 (2024).

[17]P. A. Thomas and W. L. Barnes, "Selection bias in strong coupling experiments," J. Phys. Chem. Lett. **15**, 1708–1710 (2024).
[18]R. Bhuyan, J. Mony, O. Kotov, G. W. Castellanos, J. Gómez Rivas, T. O. Shegai, and K. Börjesson, "The rise and current status of polaritonic photochemistry and photophysics," Chemical Reviews **123**, 10877–10919 (2023).
[19]E. T. Jaynes and F. W. Cummings, "Comparison of quantum and semiclassical radiation theories with to the beam maser," Proc. IEEE **51**, 89–109 (1963).
[20]M. Tavis and F. W. Cummings, "Approximate solutions for an n-molecule radiation-field hamiltonian," Phys. Rev. **188**, 692–695 (1969).
[21]P. Törmä and W. L. Barnes, "Strong coupling between surface plasmon polaritons and emitters: a review," Rep. Prog. Phys. **78**, 013901 (2015).
[22]M. Kowalewski, K. Bennett, and S. Mukamel, "Cavity femtochemistry: Manipulating nonadiabatic dynamics at avoided crossings," J. Phys. Chem. Lett. **7**, 2050–2054 (2016).
[23]H.-L. Luk, J. Feist, J. J. Toppari, and G. Groenhof, "Multiscale molecular dynamics simulations of polaritonic chemistry," J. Chem. Theory Comput. **13**, 4324–4335 (2017).
[24]J. Flick, M. Ruggenthaler, H. Appel, and A. Rubio, "Cavity born-oppenheimer approximation for correlated electron-nuclear-photon systems," J. Chem. Theory Comput. **13**, 1616–1625 (2017).
[25]T. S. Haugland, E. Ronca, E. F. Kjønstad, A. Rubio, and H. Koch, "Coupled cluster theory for molecular polaritons: Changing ground and excited states," Phys. Rev. X **10**, 041043 (2020).
[26]J. Fregoni, S. Corni, M. Persico, and G. Granucci, "Photochemistry in the strong coupling regime: A trajectory surface hopping scheme," J. Comput. Chem. **41**, 2033–2044 (2020).
[27]C. Fábri, G. J. Halász, L. S. Cederbaum, and Ágnes Vibók, "Born–oppenheimer approximation in optical cavities: from success to breakdown," Chem. Sci. **12**, 1251–1258 (2021).
[28]J. Fregoni, F. J. Garcia-Vidal, and J. Feist, "Theoretical challenges in polaritonic chemistry," ACS Photonics **9**, 1096–1107 (2022).
[29]W. Zhou, D. Hu, A. Mandal, and P. Huo, "Nuclear gradient expressions for molecular cavity quantum electrodynamics simulations using mixed quantum-classical methods," J. Chem. Phys. **157**, 104118 (2022).
[30]A. Mandal, M. Taylor, B. Weight, E. Koessler, X. Li, and P. Huo, "Theoretical advances in polariton chemistry and molecular cavity quantum electrodynamics," Chem. Rev. **123**, 9786–9879 (2023).
[31]M. Ruggenthaler, D. Sidler, and A. Rubio, "Understanding polaritonic chemistry from ab initio quantum electrodynamics," Chemical Reviews **123**, 11191–11229 (2023).
[32]T. Schwartz, J. A. Hutchison, J. Leonard, C. Genet, S. Haacke, and T. W. Ebbesen, "Polariton dynamics under strong light-molecule coupling," ChemPhysChem **14**, 125–131 (2013).
[33]J. del Pino, J. Feist, and F. J. Garcia-Vidal, "Quantum Theory of Collective Strong Coupling of Molecular Vibrations with a Microcavity Mode," New J. Phys. **17**, 053040 (2015).
[34]E. Eizner, L. A. Martínez-Martínez, J. Yuen-Shou, and S. Kéna-Cohen, "Inverting singlet and triplet excited states using strong light-matter coupling," Sci. Adv. **5**, eaax4482 (2019).
[35]P. Michetti and G. C. L. Rocca, "Polariton states in disordered organic microcavities," Phys. Rev. B. **71**, 115320 (2005).
[36]D. Morozov and G. Groenhof, "Hydrogen bond fluctuations control photochromism in a reversibly photo-switchable fluorescent protein," Angew. Chem. Int. Ed. **55**, 576–578 (2016).
[37]D. Morozov, V. Modi, V. Mironov, and G. Groenhof, "The photocycle of bacteriophytochrome is initiated by counterclockwise chromophore isomerization," J. Phys. Chem. Lett. **13**, 4538–4542 (2022).
[38]R. H. Tichauer, J. Feist, and G. Groenhof, "Multiscale simulations of molecular polaritons: the effect of multiple cavity modes on polariton relaxation," J. Chem. Phys. **154**, 104112 (2021).
[39]I. Sokolovskii, R. H. Tichauer, J. F. Dmitry Morozov, and G. Groenhof, "Multi-scale molecular dynamics simulations of enhanced energy transfer in organic molecules under strong coupling," Nat. Commun. **14**, 6613 (2023).
[40]I. Sokolovskii and G. Groenhof, "Photochemical initiation of polariton-mediated exciton propagation," Nanophotonics **13**, 2687–2694 (2024).
[41]R. H. Tichauer, D. Morozov, I. Sokolovskii, J. J. Toppari, and G. Groenhof, "Identifying vibrations that control non-adiabatic relaxation of polaritons in strongly coupled molecule-cavity systems," J. Phys. Chem. Lett. **13**, 6259–6267 (2022).
[42]J. B. Pérez-Sánchez, A. Koner, N. P. Stern, and J. Yuen-Zhou, "Simulating molecular polaritons in the collective regime using few-molecule models," Proc. Natl. Acad. Sci. USA **120**, e2219223120 (2023).
[43]E. Davidsson and M. Kowalewski, "Atom assisted photochemistry in optical cavities," J. Phys. Chem. A **124**, 4672–4677 (2020).
[44]F. C. Spano, "Exciton–phonon polaritons in organic microcavities: Testing a simple ansatz for treating a large number of chromophores," J. Chem. Phys. **152**, 204113 (2020).
[45]C. Schäfer, "Polaritonic chemistry from first principles via embedding radiation reaction," J. Phys. Chem. Lett. **13**, 6905–6911 (2022).
[46]P. Fowler-Wright, B. W. Lovett, and J. Keeling, "Efficient many-body non-markovian dynamics of organic polaritons," Phys. Rev. Lett. **129**, 173001 (2022).
[47]T. E. Li, "Mesoscale molecular simulations of fabry-pérot vibrational strong coupling," arXiv **2403.12282** (2024).
[48]J. Galego, F. J. Garcia-Vidal, and J. Feist, "Cavity-induced modifications of molecular structure in the strong-coupling regime," Phys. Rev. X **5**, 041022 (2015).
[49]M. Kowalewski, K. Bennett, and S. Mukamel, "Non-adiabatic dynamics of molecules in optical cavities," J. Chem. Phys. **144**, 054309 (2016).
[50]P. Forn-Díaz, L. Lamata, E. Rico, J. Kono, and E. Solano, "Ultrastrong coupling regimes of light-matter interaction," Rev. Mod. Phys. **91**, 025005 (2019).
[51]M. S. Rider and W. L. Barnes, "Something from nothing: linking molecules with virtual light," Contemporary Physics **62**, 217–232 (2022).
[52]R. Houdré, R. P. Stanley, and M. Ilegems, "Vacuum-field rabi splitting in the presence of inhomogeneous broadening: Resolution of a homogeneous linewidth in an inhomogeneously broadened system," Phys. Rev. A **53**, 2711–2715 (1996).
[53]L. A. Martínez-Martínez, E. Eizner, S. Kéna-Cohen, and J. Yuen-Zhou, "Triplet harvesting in the polaritonic regime: A variational polaron approach," J. Chem. Phys. **151**, 054106 (2019).
[54]P. C. T. Souza, R. Alessandri, J. Barnoud, S. Thallmair, I. Faustino, F. Grünewald, I. Patmanidis, H. Abdizadeh, B. M. H. Bruininks, T. A. Wassenaar, P. C. Kroon, J. Melcr, V. Nieto, V. Corradi, H. M. Khan, J. Domański, M. Javanainen, H. Martinez-Seara, N. Reuter, R. B. Best, I. Vattulainen, L. Monticelli, X. Periole, D. P. Tieleman, A. H. de Vries, and S. J. Marrink, "Martini 3: a general purpose force field for coarse-grained molecular dynamics," Nature Methods **18**, 382–388 (2021).
[55]J. A. Stevens, F. Grünewald, P. A. M. van Tilburg, M. König, B. R. Gilbert, T. A. Brier, Z. R. Thornburg, Z. Luthey-Schulten, and S. J. Marrink, "Molecular dynamics simulation of an entire cell," Frontiers in Chemistry **11** (2023), 10.3389/fchem.2023.1106495.
[56]G. Groenhof, C. Climent, J. Feist, D. Morozov, and J. J. Toppari, "Tracking polariton relaxation with multiscale molecular dynamics simulations," J. Chem. Phys. Lett. **10**, 5476–5483 (2019).
[57]B. Hess, C. Kutzner, D. van der Spoel, and E. Lindahl, "Gromacs 4: Algorithms for highly efficient, load-balanced, and scalable molecular simulation," J. Chem. Theory Comput. **4**, 435–447 (2008).
[58]I. Ufimtsev and T. J. Martínez, "Quantum chemistry on graphical processing units. 3. analytical energy gradients and first principles molecular dynamics," J. Chem. Theory Comput. **5**, 2619–2628 (2009).
[59]A. Titov, I. Ufimtsev, N. Luehr, and T. J. Martínez, "Generating efficient quantum chemistry codes for novel architectures," J. Chem. Theory Comput. **9**, 213–221 (2013).
[60]M. J. Frisch, G. W. Trucks, H. B. Schlegel, G. E. Scuseria, M. A. Robb, J. R. Cheeseman, G. Scalmani, V. Barone, G. A. Petersson, H. Nakatsuji, X. Li, M. Caricato, A. V. Marenich, J. Bloino, B. G. Janesko, R. Gomperts, B. Mennucci, H. P. Hratchian, J. V. Ortiz, A. F. Izmaylov, J. L. Sonnenberg, D. Williams-Young, F. Ding, F. Lipparini, F. Egidi, J. Goings, B. Peng, A. Petrone, T. Henderson, D. Ranasinghe, V. G. Zakrzewski, J. Gao, N. Rega, G. Zheng, W. Liang, M. Hada, M. Ehara, K. Toyota, R. Fukuda, J. Hasegawa, M. Ishida, T. Nakajima, Y. Honda, O. Kitao, H. Nakai, T. Vreven, K. Throssell, J. A. Montgomery, Jr., J. E. Peralta, F. Ogliaro, M. J. Bearpark, J. J. Heyd, E. N. Brothers, K. N. Kudin, V. N. Staroverov, T. A. Keith, R. Kobayashi, J. Normand, K. Raghavachari, A. P. Rendell, J. C. Burant, S. S. Iyengar, J. Tomasi, M. Cossi, J. M. Millam, M. Klene, C. Adamo, R. Cammi, J. W. Ochterski, R. L. Martin, K. Mo-

rokuma, O. Farkas, J. B. Foresman, and D. J. Fox, "Gaussian~16 Revision C.01," (2016), gaussian Inc. Wallingford CT.
[61] I. Sokolovskii and G. Goenhof, "Non-hermitian molecular dynamics simulations of exciton–polaritons in lossy cavities," J. Chem. Phys. **160**, 092501 (2024).
[62] B. A. C. Horta, P. T. Merz, P. F. J. Fuchs, J. Dolenc, S. Riniker, and P. H. Hünenberger, "A gromos-compatible force field for small organic molecules in the condensed phase: The 2016h66 parameter set," J. Chem. Theory. Comput. **12**, 3825–3850 (2016).
[63] B. Hess, H. Bekker, H. J. C. Berendsen, and J. G. E. M. Fraaije, "LINCS: A linear constraint solver for molecular simulations," J. Comput. Chem. **18**, 1463–1472 (1997).
[64] H. J. C. Berendsen, J. P. M. Postma, W. F. van Gunsteren, A. DiNola, and J. R. Haak, "Molecular dynamics with coupling to an external bath," J. Chem. Phys. **81**, 3684–3690 (1984).
[65] A. D. Becke, "A new mixing of Hartree-Fock and local density-functional theories," J. Chem. Phys. **98**, 1372 (1993).
[66] C. T. Lee, W. T. Yang, and R. G. Parr, "Development of the colle-salvet correlation-energy formula into a functional of the electron density," Phys. Rev. B **37**, 785–789 (1988).
[67] T. Yanai, D. P. Tew, and N. C. Handy, "A new hybrid exchange-correlation functional using the coulomb-attenuating method (cam-b3lyp)," Chem. Phys. Lett. **393**, 51–57 (2004).
[68] T. H. Dunning, "Basis functions for use in molecular calculations. i. contractions of (9s5p) atomic basis sets for the first-row atoms," J. Chem. Phys. **53**, 2823–2833 (1970).
[69] E. Runge and E. K. U. Gross, "Density-functional theory for time-dependent systems," Phys. Rev. Lett **52**, 997–1000 (1984).
[70] S. Hirata and M. Head-Gordon, "Time-dependent density functional theory within the tamm–dancoff approximation," Chem. Phys. Lett. **314**, 291–299 (1999).
[71] Y. Duan, C. Wu, S. Chowdhury, M. C. Lee, G. M. Xiong, W. Zhang, R. Yang, P. Cieplak, R. Luo, T. Lee, J. Caldwell, J. M. Wang, and P. Kollman, "A point-charge force field for molecular mechanics simulations of proteins based on condensed-phase quantum mechanical calculations," J. Comput. Chem. **24**, 1999–2012 (2003).
[72] W. L. Jorgensen, J. Chandrasekhar, J. D. Madura, R. W. Impey, and M. L. Klein, "Comparison of simple potential functions for simulatin liquid water," J. Chem. Phys. **79**, 926–935 (1983).
[73] G. Bussi, D. Donadio, and M. Parrinello, "Canonical sampling through velocity rescaling," J. Chem. Phys. **126**, 014101 (2007).
[74] D. Lidzey, A. Fox, M. Rahn, M. Skolnick, V. Agranovich, and S. Walker, "Experimental study of light emission from strongly coupled organic semiconductor microcavities following nonresonant laser excitation," Phys. Rev. B **65**, 195312–1 – 195312–10 (2002).
[75] G. Lodden and R. Holmes, "Electrical excitation of microcavity polaritons by radiative pumping from a weakly coupled organic semiconductor," Phys. Rev. B **82**, 125317 (2010).
[76] D. M. Coles, P. Michetti, C. Clark, W. Tsoi, A. M. Adawi, J. Kim, and D. G. Lidzey, "Vibrationally assisted polariton-relaxation processes in strongly coupled organic-semiconductor microcavities," Adv. Funct. Mater. **21**, 3691–3696 (2011).
[77] D. M. Coles, R. Grant, D. G. Lidzey, C. Clark, and P. G. Lagoudakis, "Imaging the polariton relaxation bottleneck in strongly coupled organic semiconductor microcavities," Phys. Rev. B **88**, 121303 (2013).
[78] N. Somaschi, L. Mouchliadis, D. Coles, I. E. Perakis, D. G. Lidzey, P. G. Lagoudakis, and P. G. Savvidis, "Ultrafast polariton population build-up mediated by molecular phonons in organic microcavities," Appl. Phys. Lett. **99**, 143303 (2011).
[79] V. M. Agranovich, M. Litinskaia, and D. G. Lidzey, "Cavity polaritons in microcavities containing disordered organic semiconductors," Phys. Rev. B **67**, 085311 (2003).
[80] M. Litinskaya, P. Reineker, and V. M. Agranovich, "Fast polariton relaxation in strongly coupled organic microcavities," J. Lumin. **110**, 364–372 (2004).
[81] G. Groenhof and J. J. Toppari, "Coherent light harvesting through strong coupling to confined light," J. Phys. Chem. Lett. **9**, 4848–4851 (2018).
[82] O. Vendrell, "Coherent dynamics in cavity femtochemistry: Application of the multi-configuration time-dependent hartree method," Chem. Phys. **509**, 55–65 (2018).
[83] O. Vendrell, "Collective jahn-teller interactions through light-matter coupling in a cavity," Phys. Rev. Lett. **121**, 253001 (2018).
[84] I. S. Ulusoy, J. A. Gomez, and O. Vendrell, "Modifying the nonradiative decay dynamics through conical intersections via collective coupling to a cavity mode," J. Phys. Chem. A **123**, 8832–8844 (2019).
[85] R. H. Tichauer, I. Sokolovskii, and G. Groenhof, "Tuning coherent propagation of organic exciton-polaritons through the cavity q-factor," Adv. Sci. **10**, 2302650 (2023).
[86] V. Agranovich and Y. Gartstein, "Nature and dynamics of low-energy exciton polaritons in semiconductor microcavities," Phys. Rev. B **75**, 075302 (2007).
[87] S. Takeuchi and T. Tahara, "Coherent nuclear wavepacket motions in ultrafast excited-state intramolecular proton transfer: Sub-30-fs resolved pump-probe absorption spectroscopy of 10-hydroxybenzo[h]quinoline in solution," J. Phys. Chem. A **109**, 10199–10207 (2005).
[88] C. Kim and T. Joo, "Coherent excited state intramolecular proton transfer probed by time-resolved fluorescence," PCCP **11**, 10266–10269 (2009).
[89] J. Lee, C. Kim, and T. Joo, "Active role of proton in excited state intramolecular proton transfer reaction," J. Phys. Chem. A **117**, 1400–1405 (2013).
[90] J. Kim, C. Kim, C. Burger, M. Park, M. Kling, D. Kim, and T. Joo, "Non-born–oppenheimer molecular dynamics observed by coherent nuclear wave packets," J. Phys. Chem. Lett. **11**, 755–761 (2020).
[91] D. Picconi, "Nonadiabatic quantum dynamics of the coherent excited state intramolecular proton transfer of 10-hydroxybenzo[h]quinoline," PPS **20**, 1455–1473 (2021).
[92] J. George, S. Wang, T. Chervy, A. Canaguier-Durand, G. Schaeffer, J.-M. Lehn, J. A. Hutchison, C. Genet, and T. W. Ebbesen, "Ultra-strong coupling of molecular materials: spectroscopy and dynamics," Faraday Discuss. **178**, 281–294 (2015).
[93] F. Wu, D. Finkelstein-Shapiro, M. Wang, I. Rosenkampff, A. Yartsev, T. Pascher, T. C. Nguyen-Phan, R. Cogdell, K. B. 3, and T. Pullerits, "Optical cavity-mediated exciton dynamics in photosynthetic light harvesting 2 complexes," Nat. Comm. **13**, 6864 (2022).
[94] J. Galego, F. J. Garcia-Vidal, and J. Feist, "Many-Molecule Reaction Triggered by a Single Photon in Polaritonic Chemistry," Phys. Rev. Lett. **119**, 136001 (2017).
[95] L. S. Cederbaum, "Cooperative molecular structure in polaritonic and dark states," The Journal of Chemical Physics **156**, 184102 (2022).
[96] R. T. Grant, P. Michetti, A. J. Musser, P. Gregoire, T. Virgili, E. Vella, M. Cavazzini, K. Georgiou, F. Galeotti, C. Clark, J. Clark, C. Silva, and D. G. Lidzey, "Efficient radiative pumping of polaritons in a strongly coupled microcavity by a fluorescent molecular dye," Adv. Optical Mater. **4**, 1615–1623 (2016).
[97] E. Hulkko, S. Pikker, V. Tiainen, R. H. Tichauer, G. Groenhof, and J. J. Toppari, "Effect of molecular stokes shift on polariton dynamics," J. Chem. Phys. **154**, 154303 (2021).
[98] W. J. Chang, H. Zeng, C. K. T. Weatherly, J. Provazza, P. Liu, E. A. Weiss, N. P. Stern, and R. Tempelaar, "Dark state concentration dependent emission and dynamics of cdse nanoplatelet exciton-polaritons," Chemrxiv (2024), 10.26434/chemrxiv-2024-610nl.
[99] R. Bhuyan, M. Lednev, J. Feist, and K. Börjesson, "The effect of the relative size of the exciton reservoir on polariton photophysics," Adv. Opt. Mater. **12**, 2301383 (2023).
[100] S. Felicetti, J. Fregoni, T. Schnappinger, S. Reiter, R. de Vivie-Riedle, and J. Feist, "Photoprotecting uracil by coupling with lossy nanocavities," J. Chem. Phys. Lett. **11**, 8810–8818 (2020).
[101] D. Hu and P. Huo, "Ab initio molecular cavity quantum electrodynamics simulations using machine learning models," J. Chem. Theory Comput. **19**, 2353–2368 (2023).
[102] A. Mischok, S. Hillebrandt, S. Kwon, and M. C. Gather, "Highly efficient polaritonic light-emitting diodes with angle-independent narrowband emission," Nature Photonics **17**, 393–400 (2023).
[103] S. Kéna-Cohen and S. R. Forrest, "Room-temperature polariton lasing in an organic single-crystalmicrocavity," Nat. Photonics **4**, 371–375 (2010).
[104] J. Keeling and S. Kéna-Cohen, "Bose-einstein condensation of exciton-polaritons in organic microcavities," Annu. Rev. Phys. Chem. **71**, 435–59 (2020).
[105] E. Davidsson and M. Kowalewski, "The role of dephasing for dark state coupling in a molecular tavis–cummings model," J. Chem. Phys. **159**,

044306 (2023).
[106]G. D. Scholes, C. A. Delpo, and B. Kudisch, "Entropy reorders polariton states," J. Phys. Chem. Lett. **11**, 6389–6395 (2020).
[107]D. R. Yarkony, "Nonadiabatic quantum chemistry—past, present, and future," Chem. Rev. **112**, 481–498 (2012).
[108]G. A. Worth and L. A. Cederbaum, "Beyond born-oppenheimer: Molecular dynamics through a conical intersection," Annu. Rev. Phys. Chem. **55**, 127–158 (2004).
[109]T. Azumi and K. Matsuzaki, "What does the term "vibronic coupling" mean?" Photochem. Photobiol. **25**, 315–326 (1977).
[110]R. Crespo-Otero and M. Barbatti, "Recent advances and perspectives on nonadiabatic mixed quantum-classical dynamics," Chem. Rev. **118**, 7026–7068 (2018).
[111]J. M. Lüttgens, F. J. Berger, and J. Zaumseil, "Population of exciton-polaritons via luminescent sp^3 defects in single-walled carbon nanotubes," ACS Photonics **8**, 182–193 (2021).
[112]J. B. Pérez-Sánchez and J. Yuen-Zhou, "Radiative pumping vs vibrational relaxation of molecular polaritons: a bosonic mapping approach," (2024), arXiv:2407.20594 [quant-ph].
[113]R. Chikkaraddy, B. de Nijs, F. Benz, S. J. Barrow, O. A. Scherman, E. Rosta, A. Demetriadou, P. Fox, O. Hess, and J. J. Baumberg, "Single-molecule strong coupling at room temperature in plasmonic nanocavities," Nature **535**, 127–130 (2016).
[114]J. Heintz, N. Markešević, E. Y. Gayet, N. Bonod, and S. Bidault, "Few-molecule strong coupling with dimers of plasmonic nanoparticles assembled on dna," ACS nano **15**, 14732–14743 (2021).
[115]A. Jumbo-Nogales, V. Krivenkov, K. Rusakov, A. S. Urban, M. Grzelczak, and Y. P. Rakovich, "Cross determination of exciton coherence length in j-aggregates," J. Phys. Chem. Lett. **13**, 10198–10206 (2022).
[116]K. J. Vahala, "Optical microcavities," Nature **424**, 839–846 (2003).
[117]M. Balasubrahmaniyam, A. Simkovich, A. Golombek, G. Ankonina, and T. Schwartz, "Unveiling the mixed nature of polaritonic transport: From enhanced diffusion to ballistic motion approaching the speed of light," Nat. Mater. **22**, 338–344 (2023).
[118]F. C. Spano, "Optical microcavities enhance the exciton coherence length and eliminate vibronic coupling in j-aggregates," J. Chem. Phys. **142**, 184707 (2015).
[119]D. Xu, A. Mandal, J. M. Baxter, S.-W. Cheng, I. Lee, H. Su, S. Liu, D. R. Reichman, and M. Delor, "Ultrafast imaging of coherent polariton propagation and interactions," Nat. Comm. **14**, 3881 (2023).
[120]R. Pandya, A. Ashoka, K. Georgiou, J. Sung, R. Jayaprakash, S. Renken, L. Gai, Z. Shen, A. Rao, and A. J. Musser, "Tuning the coherent propagation of organic exciton-polaritons through dark state delocalization," Adv. Sci. , 2105569 (2022).
[121]B. Cui, M. Sukharev, and A. Nitzan, "Short-time particle motion in one and two-dimensional lattices with site disorder," J. Chem. Phys. **158**, 164112 (2023).
[122]M. A. Berghuis, R. H. Tichauer, L. de Jong, I. Sokolovskii, P. Bai, M. Ramezani, S. Murai, G. Groenhof, and J. G. Rivas, "Controlling exciton propagation in organic crystals through strong coupling to plasmonic nanoparticle arrays," ACS Photonics **9**, 123 (2022).
[123]I. Sokolovskii and G. Groenhof, "Photochemical initiation of polariton-mediated exciton propagation," Nanophotonics **13**, 2687–2694 (2024).
[124]G. J. R. Aroeira, K. Kairys, and R. F. Ribeiro, "Theoretical analysis of exciton wave packet dynamics in polaritonic wires," J. Phys. Chem. Lett. **14**, 5681–5691 (2023).
[125]G. J. R. Aroeira, K. T. Kairys, and R. F. Ribeiro, "Coherent transient exciton transport in disordered polaritonic wires," Nanophotonics **13**, 2553–2563 (2024).